Title

Seasonal variation of the transport of black carbon aerosol from the Asian continent to the Arctic during the ARCTAS aircraft campaign

Journal

Journal of Geophysical Research Atmospheres, 116(5)

ISSN

0148-0227

Authors

Matsui, H
Kondo, Y
Moteki, N
et al.

Publication Date

2011

DOI

10.1029/2010JD015067

Seasonal variation of the transport of black carbon aerosol from the Asian continent to the Arctic during the ARCTAS aircraft campaign

H. Matsui,[1] Y. Kondo,[1] N. Moteki,[1] N. Takegawa,[1] L. K. Sahu,[2] Y. Zhao,[3] H. E. Fuelberg,[4] W. R. Sessions,[4] G. Diskin,[5] D. R. Blake,[6] A. Wisthaler,[7] and M. Koike[8]

Received 16 September 2010; revised 29 November 2010; accepted 30 December 2010; published 5 March 2011.

[1] Extensive measurements of black carbon (BC) aerosol were conducted in and near the North American Arctic during the Arctic Research of the Composition of the Troposphere from Aircraft and Satellites (ARCTAS) aircraft campaign in April and June–July 2008. We identify the pathways and mechanisms of transport of BC to the Arctic from the Asian continent using these data. The concentration, transport efficiency, and measured altitude of BC over the North American Arctic were highly dependent on season and origin of air parcels, e.g., biomass burning (BB) in Russia (Russian BB) and anthropogenic (AN) in East Asia (Asian AN). Russian BB air was mainly measured in the middle troposphere and caused maximum BC concentrations at this altitude in spring. The median BC concentration and transport efficiency of the Russian BB air were 270 ng m^{-3} (at STP) and 80% in spring and 20 ng m^{-3} and 4% in summer, respectively. Asian AN air was measured most frequently in the upper troposphere, with median values of 20 ng m^{-3} and 13% in spring and 5 ng m^{-3} and 0.8% in summer. These distinct differences are explained by differences in the transport mechanisms and accumulated precipitation along trajectories (APT), which is a measure of wet removal processes during transport. The transport of Russian BB air to the Arctic was nearly isentropic with slow ascent (low APT), while Asian AN air underwent strong uplift associated with warm conveyor belts (high APT). The APT values in summer were much larger than those in spring due to the increase in humidity in summer. These results show that the impact of BC emitted from AN sources in East Asia on the Arctic was very limited in both spring and summer. The BB emissions in Russia in spring are demonstrated to be the most important sources of BC transported to the North American Arctic.

Citation: Matsui, H., et al. (2011), Seasonal variation of the transport of black carbon aerosol from the Asian continent to the Arctic during the ARCTAS aircraft campaign, *J. Geophys. Res.*, *116*, D05202, doi:10.1029/2010JD015067.

1. Introduction

[2] In the Arctic, high concentrations of aerosols and reactive gases, so-called Arctic haze, occur in winter and spring because of efficient transport of pollution from mid latitudes and slow removal processes in these seasons [*Barrie*, 1986; *Shaw*, 1995]. Once these aerosols including black carbon (BC) deposit onto snow/ice surfaces, they lower surface reflectance and promote faster melting of snow/ice sheets in the Arctic, which is tightly coupled to climate effects through snow-albedo feedback [*Clarke and Noone*, 1985; *Flanner et al.*, 2007, 2009; *Hansen and Nazarenko*, 2004]. In addition, high number concentrations of aerosol in the Arctic haze lead to the enhancement of cloud longwave emissivity [*Lubin and Vogelmann*, 2006; *Garrett and Zhao*, 2006], contributing to surface warming and accelerating the melting of snow/ice. *Shindell and Faluvegi* [2009] estimated that decreasing concentrations of sulfate aerosols and increasing concentrations of BC in the Arctic have substantially contributed to rapid Arctic warming during the past three decades (1.1 ± 0.8°C).

[3] Previous studies have estimated the source regions of Arctic pollution using trajectory, regional, and global models

[1]Research Center for Advanced Science and Technology, University of Tokyo, Tokyo, Japan.
[2]Physical Research Laboratory, Ahmedabad, India.
[3]Air Quality Research Center, University of California, Davis, California, USA.
[4]Department of Meteorology, Florida State University, Tallahassee, Florida, USA.
[5]NASA Langley Research Center, Hampton, Virginia, USA.
[6]Department of Chemistry, University of California, Irvine, California, USA.
[7]Institute of Ion Physics and Applied Physics, University of Innsbruck, Innsbruck, Austria.
[8]Department of Earth and Planetary Science, Graduate School of Science, University of Tokyo, Tokyo, Japan.

0148-0227/11/2010JD015067

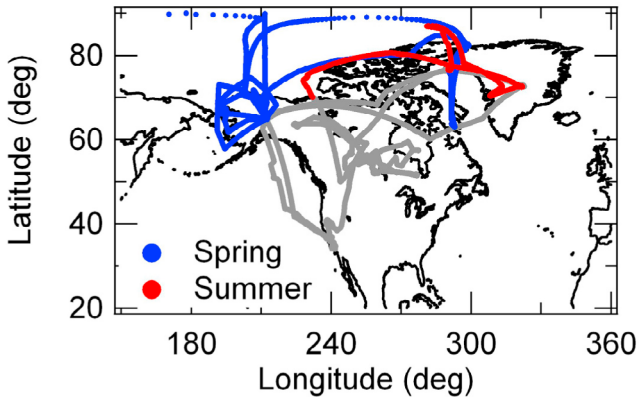

Figure 1. All flight tracks during the ARCTAS aircraft campaign (gray, blue, and red lines). Blue (spring) and red (summer) lines show the flights in and near the Arctic mainly used in this study, and we refer to these data as "Arctic data" in the text.

[e.g., *Stohl*, 2006; *Law and Stohl*, 2007; *Klonecki et al.*, 2003; *Koch and Hansen*, 2005]. Studies using trajectory [*Stohl*, 2006; *Law and Stohl*, 2007] and regional chemical transport models [*Klonecki et al.*, 2003] estimated that northern Eurasia (Europe and Siberia) is the major source of Arctic haze in the lower troposphere (LT). Aerosols and trace gases emitted from North America and Asia are uplifted during transport to the Arctic because of the large latitudinal gradient in the potential temperature. This distributes insoluble trace gases from North America and Asia at high altitudes in the Arctic. However, understanding of aerosol transport from mid latitudes to the Arctic has been poor and controversial.

[4] *Stohl* [2006] estimated that BC source contributions (for transport timescales of 5 days) from south Asia to the low-level Arctic are only 1.6% of those from Europe despite much higher emissions in south Asia. South Asian air parcels rarely reach the LT in the Arctic. In contrast, *Koch and Hansen* [2005] estimated using the Goddard Institute for Space Studies (GISS) general circulation model (GCM) that south Asia becomes the dominant source region of BC in the upper troposphere (UT) (30–50%) in the Arctic and also contributes significantly to Arctic haze near the surface. *Shindell et al.* [2008] conducted a multimodel comparison of aerosol transport to the Arctic and showed large differences in the calculated BC concentrations in the Arctic by the different GCM models used in the IPCC report. They suggested that the large differences are likely due to the different treatments of aerosol aging from hydrophobic to hydrophilic and rainout/washout processes of aerosols during transport in the individual models rather than differences in dry transport or local Arctic removal processes. This indicates the necessity of an improved understanding of the removal processes of BC during long-range transport for improved assessments of the impact of BC on the climate of the Arctic.

[5] BC particles are emitted from combustion of anthropogenic fossil fuel (AN) and biomass burning (BB). BB emissions have been shown to be important sources of BC in the Arctic, especially from late spring to summer [*Stohl et al.*, 2006, 2007; *Hsu et al.*, 1999; *Iziomon et al.*, 2006; *Paris et al.*, 2009; *Eck et al.*, 2009; *Treffeisen et al.*, 2007; *Kim et al.*, 2005; *Engvall et al.*, 2009]. *Stohl* [2006] estimated that the contributions of BC from BB, particularly from fires in Siberia, were larger than those of anthropogenic BC in summer. *Warneke et al.* [2009] observed high amounts of BC originating from Siberian and Kazakhstan BB in spring 2008 during the Aerosol, Radiation, and Cloud Processes affecting Arctic Climate (ARCPAC) aircraft campaign. *Warneke et al.* [2010] estimated that Russian BB could more than double the aerosol concentrations in Arctic haze in the winter months, although Arctic haze had been recognized to form mainly from anthropogenic emissions and their accumulation in winter and early spring. Therefore, it is important to quantify the relative contributions of AN and BB to Arctic BC in different seasons.

[6] BC measurements have been conducted at various surface stations in the Arctic (e.g., Alert in Canada, Barrow in Alaska, and Janiskoski in Russia), and seasonal variations and long-term trends of aerosols including BC have been examined [e.g., *Sirois and Barrie*, 1999; *Polissar et al.*, 1999; *Sharma et al.*, 2002, 2004, 2006; *Quinn et al.*, 2002, 2007, 2008; *Gong et al.*, 2010; *Eleftheriadis et al.*, 2009; *Huang et al.*, 2010]. However, because data from these studies are limited to the surface, the understanding of the sources, transport pathways and removal processes, and distributions of BC in the entire troposphere is very limited. The NASA Arctic Research of the Composition of the Troposphere from Aircraft and Satellites (ARCTAS) aircraft campaign was conducted in spring and summer 2008 in the Arctic [*Jacob et al.*, 2010]. As compared with previous aircraft campaigns in the Arctic [*Shipham et al.*, 1992; *Baumgardner et al.*, 2004; *Yamanouchi et al.*, 2005], much more accurate, extensive, and high-time resolution measurements of BC were conducted at various altitudes from the boundary layer (BL) to the UT in the Arctic in spring and summer.

[7] In this study, we focus on BC transport from the Asian continent (Russia and East Asia (China, Japan, and Korea)) to the Arctic because the ARCTAS measurements were made mainly over the Alaskan region, which received BC mostly originating from Asia [*Fuelberg et al.*, 2010]. We have identified important regions and fuel types (AN and BB sources) of BC sources from the Asian continent and quantify their contributions to BC over the North American Arctic using the ARCTAS data set. We have also quantified the pathways and efficiencies of BC transport from different sources in the Asian continent and used them to interpret the vertical profiles and seasonal variations of BC.

2. Measurements and the Methods of Analysis

2.1. ARCTAS Observations

[8] The measurements of BC and other related species were made on board the NASA DC-8 aircraft during the ARCTAS aircraft campaign conducted in April and June–July 2008 as a part of the international POLARCAT program of field observations of Arctic atmospheric composition during the 2007–2008 International Polar Year (Table 1). An overview of the ARCTAS campaign and meteorological conditions during the observation periods have been given by *Jacob et al.* [2010] and *Fuelberg et al.* [2010], respectively. Figure 1 shows all the flight tracks of the DC-8 aircraft

Table 1. ARCTAS Data Sets Used in This Study

Species	Instrument[a]	PI	Reference
BC	SP2	Y. Kondo (University of Tokyo)	*Moteki and Kondo* [2007, 2010]
CO	TDLAS	G. Diskin (NASA Langley)	*Sachse et al.* [1987]
CH_2Cl_2	WAS-GC	D. Blake (University of California, Irvine)	*Blake et al.* [2003]
CH_3CN	PTR-MS	A. Wisthaler (University of Innsbruck)	*Wisthaler et al.* [2002]

[a]SP2, TDLAS, WAS-GC, and PTR-MS denote single particle soot photometer, tunable diode laser absorption spectroscopy, whole air sampling–gas chromatography, and proton transfer reaction–mass spectrometry, respectively.

during the ARCTAS campaign. Flights were conducted mainly over Alaska in April (ARCTAS-A) and over western Canada in June–July (ARCTAS-B). In this study, we used 1 min average flight data observed in and near the Arctic: 5 flights (F06–10) in April and 2 flights (F21–22) in July, which are shown in Figure 1 by blue and red lines (we refer them as "Arctic data," hereafter), respectively. All the data obtained over Alaska were used for the present analysis, including those obtained at latitudes <70°N, because the Alaskan region is one of the major inflow regions of pollutants from Asia to the Arctic [e.g., *Fuelberg et al.*, 2010]. Since this study focuses on long-range transport of BC, periods sometimes strongly influenced by local forest fires in Canada were excluded in this analysis (<70°N data in F21). These air parcels were identified by trajectory calculations (transported from North America) and high acetonitrile mixing ratio (>100 ppbv), which are shown later in this section. We also excluded data in the stratosphere (ozone mixing ratio >120 ppbv) and in clouds (liquid or ice water contents >0.01 g m^{-3}). Arctic data covered the whole troposphere, and the data were not substantially biased vertically except for the lower tropospheric data in summer.

[9] The number and mass size distributions of BC were measured by a Single Particle Soot Photometer (SP2) with high accuracy and temporal resolution [*Moteki and Kondo*, 2007]. Detailed descriptions of the SP2 used during the ARCTAS campaign are given elsewhere [*Moteki and Kondo*, 2010; *Kondo et al.*, 2011a, 2011b]. The SP2 derives masses of individual BC particles with the mass equivalent diameters between 80–860 nm by measuring the intensity of laser-induced incandescence (LII) signals [*Kondo et al.*, 2011b]. The absolute accuracy of the BC measurements is estimated to be about 10% [*Kondo et al.*, 2011a]. The volume mixing ratio of carbon monoxide (CO) was measured by a Tunable Diode Laser Absorption Spectroscopy (TDLAS) instrument [*Sachse et al.*, 1987], and we used it as a tracer of polluted air parcels within the timescale of transport relevant to this study (less than 10 days). The volume mixing ratios of acetonitrile (CH_3CN) and dichloromethane (CH_2Cl_2) were measured by Proton Transfer Reaction–Mass Spectrometry (PTR-MS) and Whole Air Sampling–Gas Chromatography (WAS-GC), respectively [*Blake et al.*, 2003; *Wisthaler et al.*, 2002]. These species have often been used as tracers of BB and AN sources, respectively [e.g., *Warneke et al.*, 2006; *Chen et al.*, 2007]. Temporal linear interpolation was performed for the periods when either or both of these two species were not available to maintain a sufficient amount of data for statistical analysis.

[10] The lifetimes of CO, CH_3CN, and CH_2Cl_2 are longer than 1 month in the atmosphere. This is reflected in their variabilities with timescales longer than a month. We derived the background concentrations of these species in order to extract short-term temporal variability (less than 10 days). We represent the short-term variability by the differences between the measured and background concentrations of these species, denoted ΔCO, ΔCH_3CN, and ΔCH_2Cl_2 for the present analysis. The background concentrations of these species were defined as the lowest 5th percentiles of all ARCTAS data for every 10 K potential temperature range for each species and season, and they were linearly interpolated vertically. This method is similar to previous studies [*Koike et al.*, 2003]. Zero background concentration was assumed for BC.

[11] In this study, the BC/ΔCO ratio was used as an indicator of the transport efficiency of BC, denoted TE_{BC}, during transport from sources to the Arctic. A similar method was used previously to study the transport efficiency of aerosols [*Park et al.*, 2005; *Koike et al.*, 2003; *Garrett et al.*, 2010]. The data with $\Delta CO > 20$ parts per billion by volume (ppbv) were used for the statistical analysis. The units of the BC/ΔCO ratio are ng at standard temperature and pressure (STP) m^{-3} $ppbv^{-1}$.

[12] We note that the measurements during ARCTAS may be biased to some extent and not completely representative of the Arctic because the ARCTAS flights targeted pollution transport events. However, as we show in section 5, satellite-derived column amounts of CO and AOD during the ARCTAS-A and ARCTAS-B campaigns were similar to monthly averages for individual months over the Alaskan Arctic (the region including both measurements and transport pathways of measured air parcels), suggesting that ARCTAS data are representative of the North American Arctic in April and July 2008.

2.2. Backward Trajectories

[13] Ten day backward trajectories were released at 1 min intervals along the flight tracks using a kinematic model [*Fuelberg et al.*, 2010, and references therein] to identify the source regions of pollutants in measured air parcels. The meteorological data were from runs of the Weather Research and Forecasting (WRF) model [*Skamarock et al.*, 2008] with a horizontal resolution of 45 km and 50 vertical layers [*Fuelberg et al.*, 2010]. In this study, the source regions were defined as the BL from surface to 700 hPa (about 3 km above ground level) over four horizontal regions shown in Figure 2: Europe, Russia, Asia (excluding Russia), and North America. The altitude of 3 km is an approximate height of the upper boundary of the BL over the land during daytime. The origins of the measured air parcels were classified into 7 categories: Europe, Russia, Asia, and North America, Russia+Asia (R+A), Russia+Europe (R+E), and other, based on the trajectory calculations. For trajectories passing over only a single source region within 10 days, the corresponding air parcels were classified as Europe, Russia,

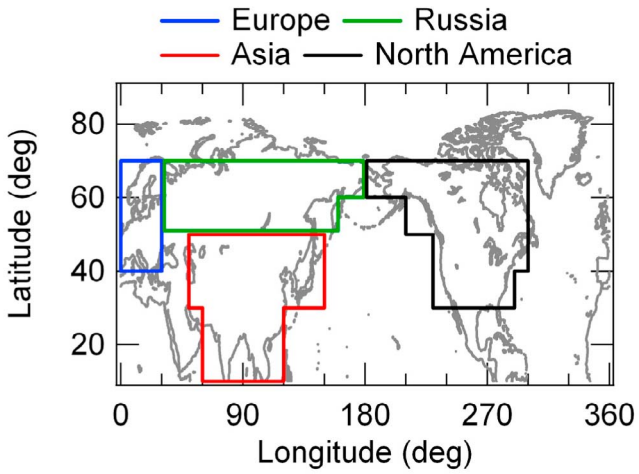

Figure 2. Source regions (Europe, Russia, Asia, and North America) defined in this study.

Asia, or North America. For trajectories passing two regions, e.g., Russia and Europe or Asia, air parcels were categorized as Russia+Europe or Russia+Asia.

[14] We calculated accumulated precipitation along individual trajectories (APT) using Global Precipitation Climatology Project (GPCP) global precipitation data [*Huffman et al.*, 2001; *Adler et al.*, 2003]. The GPCP data were derived solely from observations based on gauge measurements and geostationary and polar orbiting satellite estimates of rainfall. We used daily data with a horizontal resolution of 1 × 1 degree (1DD) [*Huffman et al.*, 2001]. The GPCP 1DD data were estimated using the Threshold-Matched Precipitation Index (TMPI), which estimates precipitation from infrared radiometers on geostationary satellites, for the latitudes 40°N–40°S and a rescaled Television Infrared Observation Satellite Program (TIROS) Operational Vertical Sounder (TOVS) from polar orbiting satellites for the higher latitudes [*Huffman et al.*, 2001]. Both were designed to sum to the GPCP satellite-gauge combined monthly precipitation estimates, which include gauge data. The amount of precipitation was summed up (accumulated) along individual trajectories from measured points to the time when each trajectory reached one of the source regions (t hours before the measurements, dependent on trajectories) and a further 48 h within the sources, because air parcels may have already been influenced by precipitation within the source regions. Therefore, the integration period for calculating the APT was t + 48 h (<10 days). We used the APT data as a measure of wet removal processes during transport. The period length of 48 h was chosen subjectively, but the results obtained in this study do not change qualitatively even if we use periods of 24 or 0 h. In fact, the correlation coefficients (R^2) of the APT data between t + 48 h with those for t + 24 and t hours were 0.98 and 0.92, respectively, for all ARCTAS data. The uncertainties in the estimates of source regions and APT were calculated by using two trajectory calculation methods and three precipitation data. One method is the model of *Fuelberg et al.* [2010] with meteorological data from the WRF model, and the other is the NIPR trajectory model [*Tomikawa and Sato*, 2005] combined with NCEP Final Operational Global Analysis (FNL) data. Three precipitation data sets are GPCP data, Climate prediction center Merged Analysis of Precipitation (CMAP) data [*Xie and Arkin*, 1997], and WRF model calculations (Appendix A). These comparisons show that the general features of the statistics and conclusions obtained in this study do not change with the choice of trajectory model or meteorological and precipitation data sets, despite the large differences in the methodologies used in deriving these data sets (measurement-based and model calculations) as well as their horizontal and temporal resolutions.

2.3. Anthropogenic and Biomass Burning Plumes

[15] As shown in Figure 3, the types of combustion for polluted air parcels were classified into AN and BB according to the concentrations of trace hydrocarbon species CH_2Cl_2 and CH_3CN. CH_2Cl_2 is emitted from industrial solvents but not produced by combustion [*Chen et al.*, 2007; *Choi et al.*, 2003]. However, we used it as a tracer of anthropogenic sources of CO and BC, because solvent (CH_2Cl_2) and combustion (CO) sources generally coexist in urban areas at the horizontal scale of this study. CH_3CN is known to be a useful tracer for BB emissions [*de Gouw et al.*, 2004; *Warneke et al.*, 2004, 2006]. AN-impacted air parcels were defined as those with $\Delta CH_2Cl_2 > 5$ pptv and $\Delta CH_3CN < 100$ pptv (red area in Figure 3). BB-impacted air parcels were similarly defined as those with $\Delta CH_3CN > 50$ pptv and $\Delta CH_2Cl_2 < 10$ pptv (green area in Figure 3). Air parcels with high ΔCH_2Cl_2 and ΔCH_3CN were influenced by both AN and BB sources, and they are denoted ANBB. Low-ΔCH_2Cl_2 and ΔCH_3CN air parcels represent background air (BG).

[16] Tables 2a and 2b contain the numbers of the data points in different categories obtained during the ARCTAS-A and ARCTAS-B periods, respectively. The sources of about 75% of the data were not identified, because about 50 and 60% of Arctic data were classified in source region of

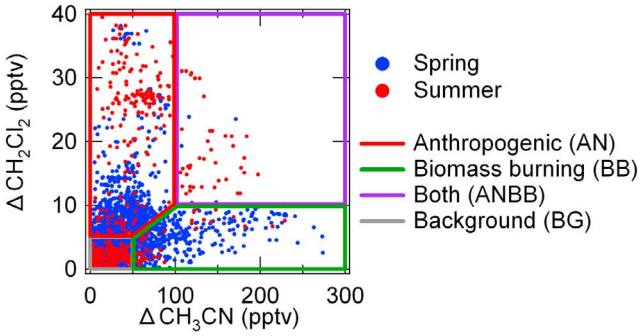

Figure 3. Diagrams for air parcel classification by fuel type. The sources of anthropogenic (AN), biomass burning (BB), anthropogenic and biomass burning (ANBB), and background (BG) were defined based on the mixing ratios of ΔCH_2Cl_2 and ΔCH_3CN, which are tracers of anthropogenic and biomass burning sources, respectively. ΔA denotes the difference between measured and background concentration for species A (see section 2.1 for details). Blue and red circles are 1 min average data in spring and summer (Arctic data), respectively.

Table 2a. Data Point Number and Fraction of Air Parcels From Individual Sources During the ARCTAS-A (Spring) Campaign

Source Region	AN	BB	ANBB	Total	Fraction (%)
Europe	27	7	0	34	6.9
Russia + Europe	33	29	2	64	13.0
Russia	38	75	0	113	23.0
Russia + Asia	17	37	3	57	11.6
Asia	73	4	0	77	15.7
North America	132	14	0	146	29.7
Total	320	166	5	491	100.0

"other" and source type "BG," respectively. We used only the source-identified data listed in Tables 2a and 2b, because we focus on air parcels substantially influenced by AN and BB emissions within 10 days prior to measurement. Within the source-identified air, the fraction of AN and BB air parcels were 65 and 34% in the springtime and 73 and 12% in the summertime (the other is ANBB air parcels), respectively. Air parcels transported from Europe and Asia were mainly influenced by AN, while those from Russia were generally impacted by BB.

[17] The biggest assumption used in this study is that a measured air parcel can be classified into one representative source region and process. This assumption is reasonable in some cases because individual source regions in this study are sufficiently large and the numbers of air parcels near the boundary of definitions between AN and BB sources were relatively small (Figure 3). In the real atmosphere, air parcels can be influenced by various source regions and fuel types, especially when the transit period is relatively long.

3. Sources, Transport, and Removal of BC in Spring

3.1. Case Study (Flight 8)

[18] In this section, we describe the pathways and efficiencies of BC transport from individual source categories during the ARCTAS-A campaign.

[19] Figure 4 shows a time series plot of Flight 8 conducted over the Alaskan region on 12 April. Measured altitude (pressure) and ΔCO and BC concentrations are shown with the identified source regions and types of fuels. In the Russian BB air parcels, ΔCO and BC were high and well correlated, while in the Asian AN air parcels ΔCO was enhanced often with little changes in BC.

[20] Figure 5a shows 10 day backward trajectories of Asian AN air parcels for the periods indicated by the red arrow in Figure 4. The numbers in Figure 5a denote air parcel locations of 1, 2, and 3 days before the measurements, respectively. Figure 5b shows potential temperature during transport for the same Asian AN air parcels. Figures 5c and 5d show the precipitation distribution from GPCP data and sea level pressure from NCEP-FNL data for the time 3 days before the measurements (9 April). The marked increase in potential temperature during the transport indicates that the Asian air parcels shown here experienced considerable nonadiabatic processes, namely condensation of water vapor and precipitation (Figure 5b). In fact, heavy precipitation was seen in the same regions 3 days before the measurements (Figure 5c). These Asian AN air parcels experienced rapid ascent from the warmer side of cold fronts associated with two low-pressure systems shown in Figure 5d and were transported northeastward and reached the Alaskan region within a few days (Figure 5a) with a substantial increase in potential temperature during ascent. These transport pathways are frequently seen in this region and season by warm conveyor belt (WCB) transport [*Eckhardt et al.*, 2003; *Oshima et al.*, 2004]. High ΔCO and low BC concentrations (low BC/ΔCO ratio) for these Asian air parcels are interpreted as resulting from WCB transport, which causes heavy precipitation leading to efficient BC removal.

[21] Figure 6 shows the trajectories and meteorological conditions for the Russian BB air parcels indicated by green arrows in Figure 4. Figures 6c and 6d show the data for the time 4 days before the measurements (8 April). These air parcels experienced much smaller potential temperature changes and precipitation amounts during transport (Figures 6b and 6c), as compared with the Asian AN air parcels (Figure 5). This is mainly because these Russian air parcels were transported from higher latitudes, where water vapor concentrations were much lower than those of Asian air parcels. In addition, there are no distinct low-pressure systems at the surface around the trajectories of these Russian BB air parcels, although a weak low-pressure region was seen at the 700 hPa level around 60°N (Figure 6d). As a result, these Russian BB air parcels were transported to the Alaskan region almost isentropically with very slow ascent (Figure 6a). Note that the altitude of air parcels was already high (around 700 hPa) in the source regions (Figure 6a), and this may be due to the higher injection height of Russian BB plumes, as shown by *Kondo et al.* [2011b]. The high BC and ΔCO concentrations (high BC/ΔCO ratio) for the Russian BB air parcels are consistent with the low precipitation amounts.

3.2. Transport Pathway and Efficiency

[22] The differences in transport pathways and TE_{BC} between the Asian AN and Russian BB air parcels were seen for the entire ARCTAS-A period in April. Figure 7a shows the GPCP mean precipitation distribution before (3–7 April) and during the ARCTAS-A period (8–17 April). A period before the campaign is included, considering the transport time from the sources to the measurement locations. Figures 7b–7d show the trajectories of the AN air parcels from Asia (Asian AN and Russia+Asia AN), BB air parcels from Russia (Russian BB, Russia+Europe BB, and Russia+Asia BB), and all source-identified data, respectively, during the ARCTAS-A period, together with the precipitation intensity. Trajectories of almost all AN air parcels from Asia and BB air parcels from Russia were similar to

Table 2b. Data Point Number and Fraction of Air Parcels From Individual Sources During the ARCTAS-B (Summer) Campaign

Source Region	AN	BB	ANBB	Total	Fraction (%)
Europe	0	0	0	0	0
Russia + Europe	0	0	0	0	0
Russia	8	9	10	27	17.0
Russia + Asia	78	3	13	94	59.1
Asia	27	0	2	29	18.2
North America	2	7	0	9	5.7
Total	115	19	25	159	100.0

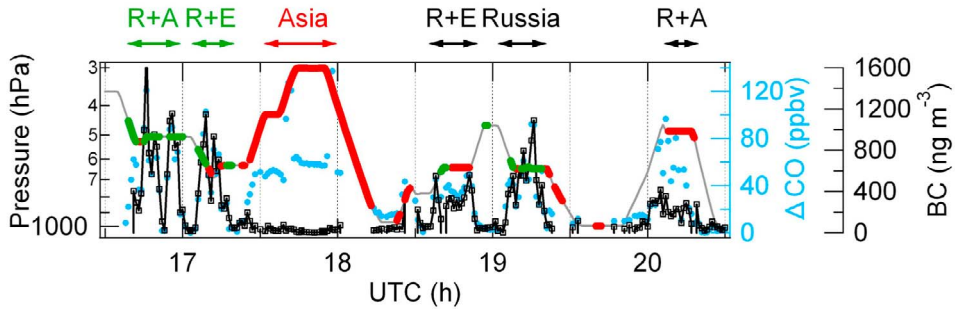

Figure 4. Time series plot of the data from Flight 8, conducted over the Alaskan region. Pressure (gray line, left axis), ΔCO (light blue circles, right axis), and BC (black line with open squares, right axis) are shown with the identification of the source regions and fuel types. R+A (Russia and Asia), R+E (Russia and Europe), Asia, and Europe are representative source regions of measured air parcels during the period of individual arrows. Green and red lines indicate air parcels impacted by biomass burning and anthropogenic emissions, respectively.

those discussed in section 3.1. Namely, most AN air parcels from Asia experienced rapid ascent on WCBs associated with heavy precipitation near the source regions. Most Russian BB air parcels experienced slower ascent and much less precipitation than the Asian AN air parcels. The trajectories (transport pathways and altitudes) and precipitation shown in Figures 7b and 7c are considered to be typical in the springtime because these Asian AN and Russian BB air parcels were found in all five flights (F06–10) and in four flights (F07–10), respectively.

[23] As shown in Figure 7d, we sampled almost no air parcels from south Asian sources (<30°N) during ARCTAS-A. In addition, TE_{BC} from south Asia (<30°N) should be lower than that from Asian AN (30°–50°N) due to heavier precipitation. Considering these, the contribution of BC from south Asia to the Arctic must be very limited.

[24] Figure 8a shows a scatterplot between the BC/ΔCO ratio and APT for all Arctic data and those for individual source regions and fuel types. On average, the BC/ΔCO ratio decreased with increasing APT, indicating that BC removal by precipitation is one of the most important processes in controlling BC concentrations in the Arctic. The BC/ΔCO ratio was low and APT was high for Asian AN air parcels. By contrast, the BC/ΔCO ratio was much higher for Russian BB air parcels with low APT, similar to the case study discussed in section 3.1. The BC/ΔCO ratios of AN-impacted air (Asia, Europe and North America) with higher APT were lower than those for BB-impacted air (Russia, Russia+Europe and Russia+Asia), on average. An exception is AN-impacted air from Russia+Asia, with a moderately high median BC/ΔCO ratio (purple circle). These air parcels were transported to the Arctic with slow ascent and low precipitation along more northerly trajectories (along the coastal region) than the Asian AN air parcels. Although the number of data points was only a quarter of that of the Asian AN air (Table 2a), Russia+Asia AN air parcels might have transported BC more effectively from East Asia to the Arctic than Asian AN air, which experienced efficient removal of BC. However, we cannot separate the sources of Russia+Asia air parcels into East Asia or Russia with the low spatial resolution of the source identification by the current trajectory-based method.

[25] Figure 8a (left) also shows the median BC/ΔCO ratios for APT < 5 mm for AN (Europe, Asia, Russia+Asia, and North America) and BB (Russia, Russia+Europe, and Russia+Asia) air parcels. The number of data points with APT < 5 mm is 337 and 163 for AN and BB air parcels, respectively. They are considered representative of the BC/ΔCO ratios in the source regions (minimum impact of wet removal processes) and denoted $[BC/\Delta CO]_{source}$. A $[BC/\Delta CO]_{source}$ ratio of 3.3 for AN air parcels was derived mainly from North American air parcels, because there are few Asian and European air data with APT < 5 mm. The $[BC/\Delta CO]_{source}$ ratio of 7.6 for BB air was derived mostly from the Russian (Russia, Russia+Europe, and Russia+Asia) air data. The difference in the $[BC/\Delta CO]_{source}$ ratios between the AN and BB impacted air by a factor of 2.5 is consistent with previous studies [*Warneke et al.*, 2009; *Kondo et al.*, 2011b]. For fossil fuel combustion, the BC/CO emission ratio was estimated to be 3.2 ± 1.0 in California [*Kondo et al.*, 2011b]. For BB, the BC/CO emission ratio was estimated to be 8.7 ± 3.7 for Russia [*Kondo et al.*, 2011b] and 10 ± 5 for Kazakhstan and 7 ± 4 for Lake Baikal [*Warneke et al.*, 2009].

[26] We calculated $TE_{BC,\,t}$, the transport efficiency of BC at time t, using equation (1).

$$TE_{BC,t} = \frac{[BC/\Delta CO]_t}{[BC/\Delta CO]_{source}} \quad (1)$$

In this equation, $[BC/\Delta CO]_t$ is the BC/ΔCO ratio at time *t*. Different $[BC/\Delta CO]_{source}$ values were used for the AN and BB sources. Tables 3a and 3b show the median TE_{BC} for different air parcel categories. Figure 8b shows the correlation of TE_{BC} with APT. The median TE_{BC} for Asian AN was as low as 13%, and TE_{BC} for the Russian BB air was as high as 83%. The magnitude of the difference in TE_{BC} between the two regions is remarkable, considering they represent values for the same season.

[27] According to the field measurements over the East Asian region [*Han et al.*, 2009; *Matsui et al.*, 2009; N. Oshima et al., manuscript in preparation, 2011; R. Verma et al., manuscript in preparation, 2011], the average BC/CO emission ratios were considered to be about 4–7. These values are about a factor of 1.5 to 2 greater than the [BC/

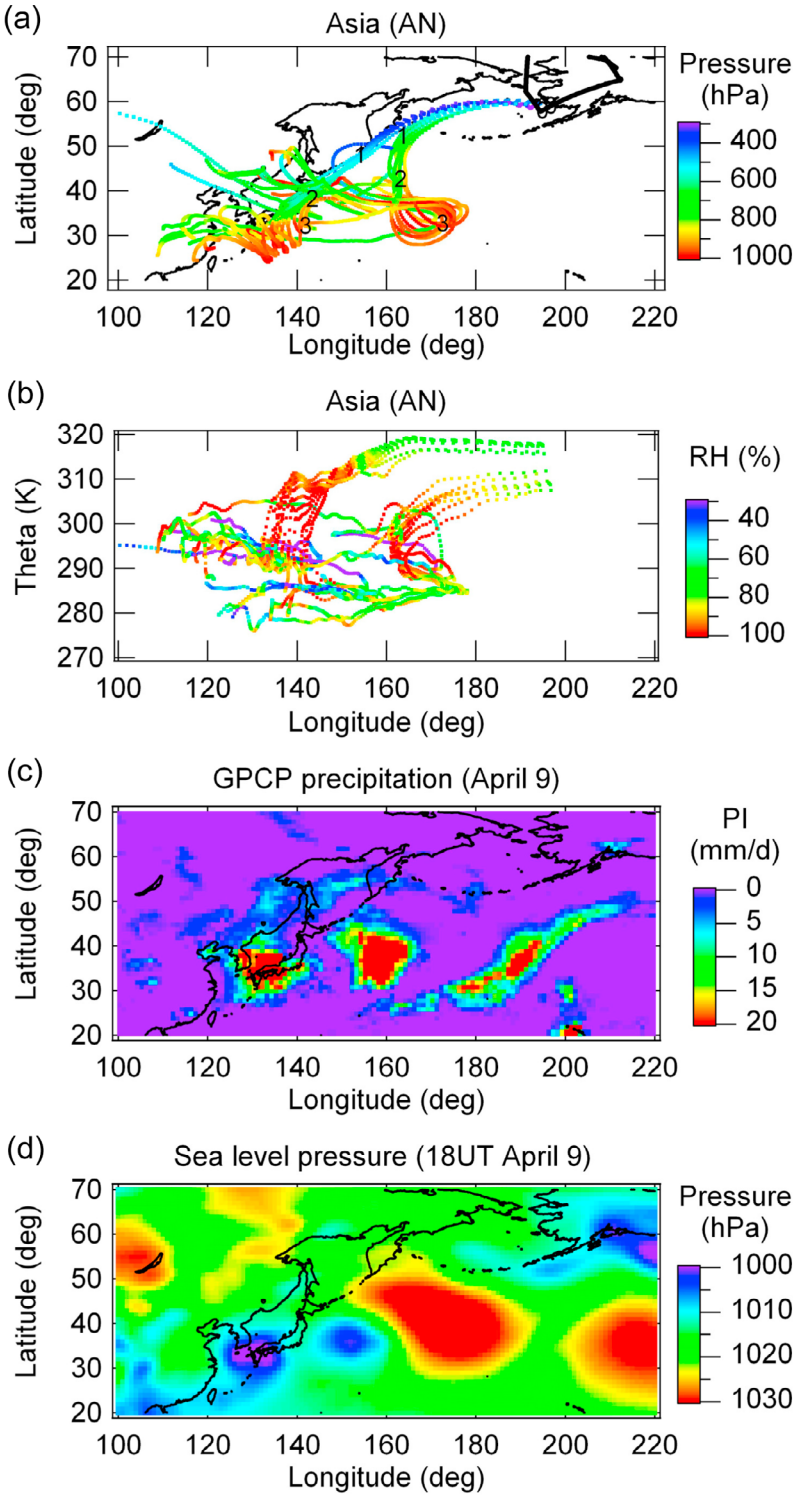

Figure 5. (a) Ten day backward trajectories of air parcels impacted by anthropogenic emissions in Asia (the period indicated by the red arrow in Figure 4). The numbers show the locations of the air parcels 0–3 days prior to their measurement during Flight 8. (b) Changes in the potential temperature along trajectories of the same air parcels. (c) Daily precipitation distribution on 9 April (3 days before Flight 8) derived from GPCP data. PI denotes precipitation intensity (mm/d). (d) Sea level pressure at 1800 UT on 9 April derived from NCEP-FNL data.

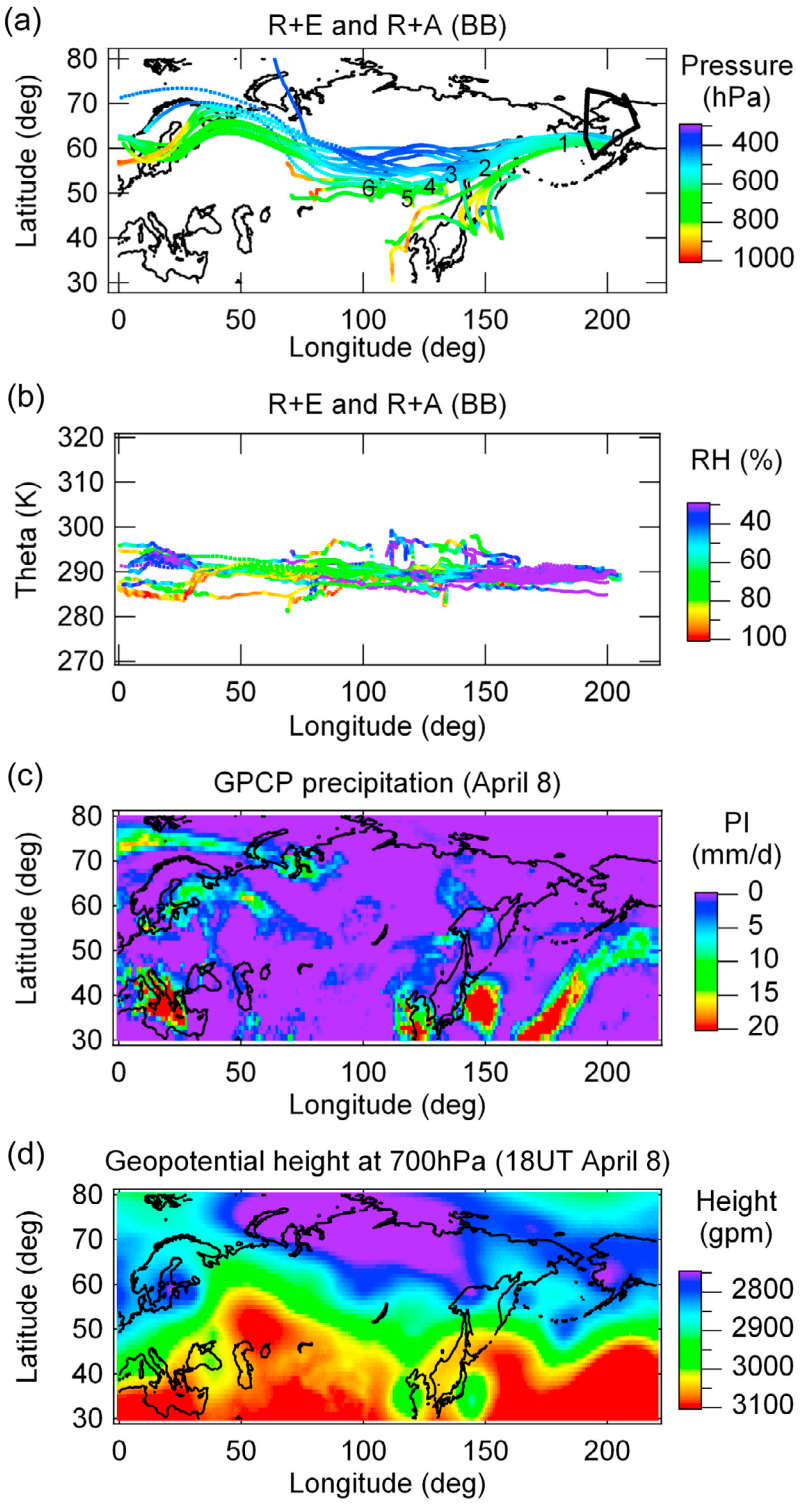

Figure 6. (a) Ten day backward trajectories of the air parcels impacted by biomass burning in Russia (R+E and R+A, the period indicated by the green arrows in Figure 4). The numbers show the locations of the air parcels 0–6 days prior to their measurement during Flight 8. (b) Changes in the potential temperature along trajectories of the same air parcels. (c) Daily precipitation amounts on 8 April (4 days before Flight 8) derived from GPCP data. PI denotes precipitation intensity (mm/d). (d) Geopotential height at 700 hPa at 1800 UT on 8 April derived from NCEP-FNL data.

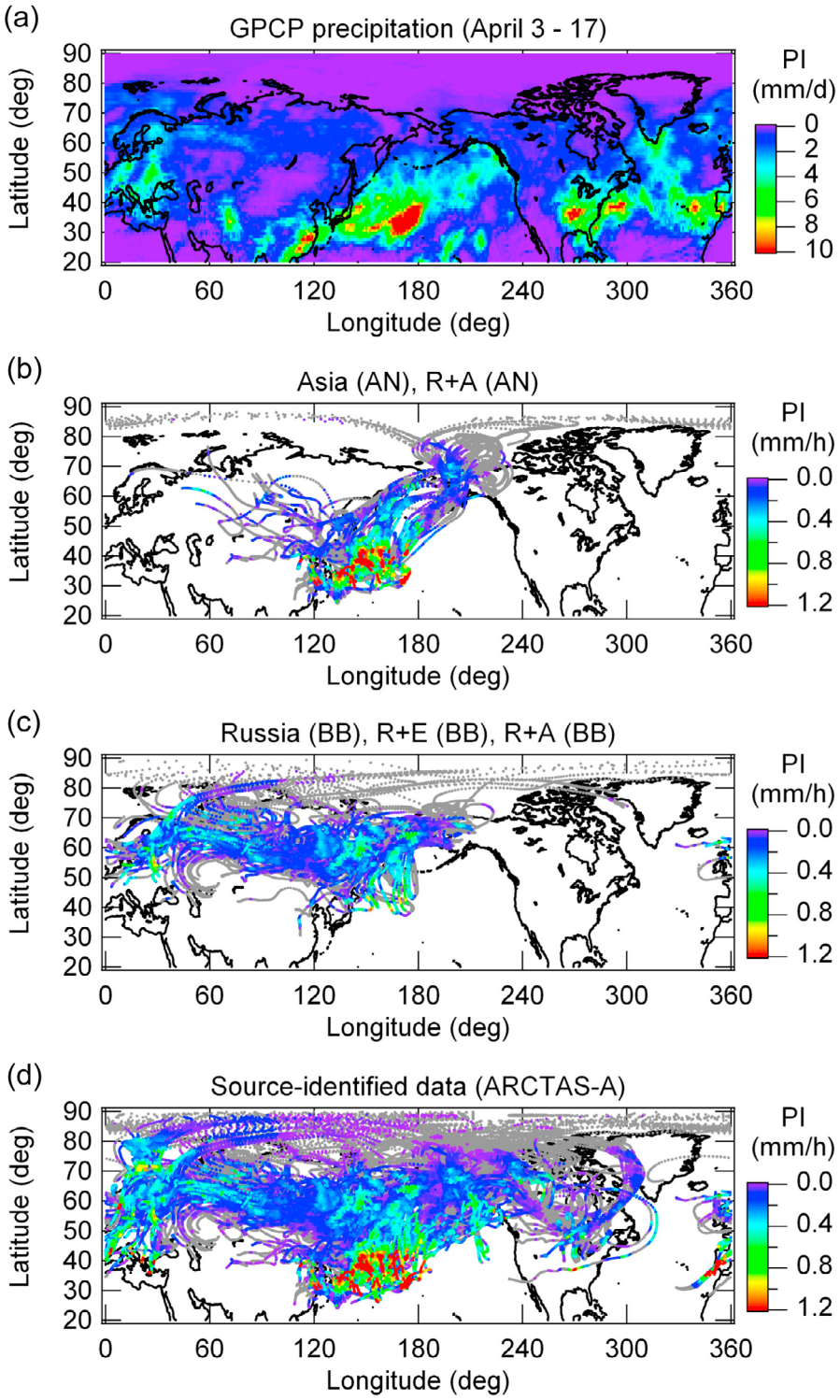

Figure 7. (a) Average precipitation distribution before (3–7 April) and during the ARCTAS-A campaign (8–17 April). A period before the campaign was included considering the transport time from the sources to the locations of the measurement. Ten day backward trajectories are shown for (b) anthropogenic air parcels from Asia (Asia and R+A), (c) biomass burning air parcels from Russia (Russia, R+E, and R+A), and (d) all source-identified air parcels (see the definition in section 2.3) during the ARCTAS-A campaign. PI denotes precipitation intensity. The periods when PI < 0.01 mm/h are shown with gray dots.

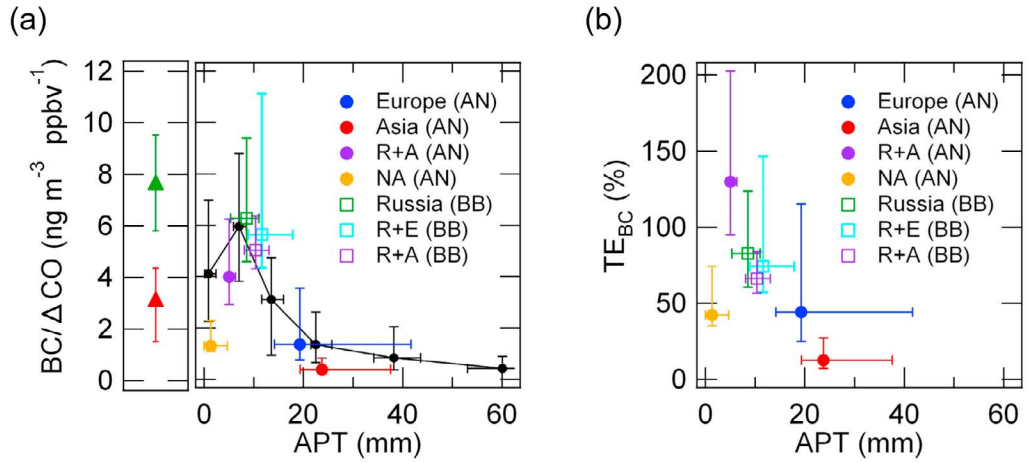

Figure 8. Scatterplots of (a) BC/ΔCO ratio and (b) transport efficiency of BC (TE_{BC}) as a function of accumulated precipitation along trajectories (APT, see section 2.2) during the ARCTAS-A campaign. The medians (circles or squares with color) and the 25th to 75th percentiles (horizontal and vertical bars) are shown for different source regions and fuel types. The black line in Figure 8a shows the relationship between the BC/ΔCO ratio and APT for all the Arctic data in spring (Flights 6–10). Red and green triangles (Figure 8a, left) and their bars show the medians and 25th to 75th percentiles of the BC/CO emission ratios for fossil fuel combustion (AN) and biomass burning (BB), respectively. These values were estimated using all source-identified air parcels with APT < 5 mm. The definition of TE_{BC} is described by equation (1) in section 3.2.

$\Delta CO]_{source}$ ratio for AN. Therefore, the TE_{BC} of 13% for the Asian AN air is likely to be an overestimate. Similarly, TE_{BC} for AN-impacted air from Russia+Asia exceeded 100% due to the uncertainty in the BC/ΔCO emission ratio.

[28] Because of the distinct differences in TE_{BC} and $[BC/\Delta CO]_{source}$ between the AN- and BB-impacted air, the relative contributions of BB is larger for BC than for ΔCO to their abundances in the North American Arctic. We calculated the contributions of individual sources to the total BC and ΔCO amounts in the North American Arctic (sum of the concentration for all source-identified data) by the following equation.

$$F_{A,i} = \frac{\sum_t C_{A,i,t}}{\sum_j \sum_t C_{A,j,t}} \quad (2)$$

$F_{A,i}$ is the fractional contribution of source i to the total amount of species A in the North American Arctic, expressed

Table 3a. Measured and Estimated Statistics of Air Parcels From Individual Sources During the ARCTAS-A (Spring) Campaign

Sources	AN or BB	N	Pressure[a] (hPa)	ΔCO[a] (ppbv)	BC[a] (ng m^{-3})	APT[a,b] (mm)	TE_{BC}[a,c] (%)	$F_{\Delta CO}$[c] (%)	F_{BC}[c] (%)
Europe	AN	27	479	38.3	48.2	19.3	44.2	5.1	2.6
	BB	7	488	66.7	272	17.4	65.5	2.7	3.4
R+E	AN	33	489	34.4	104	11.0	110	6.5	6.5
	BB	29	566	53.8	312	11.6	74.3	9.3	13.2
	ANBB	2	441	64.4	255	17.3	49.1	0.74	0.64
Russia	AN	38	614	22.2	96.4	5.5	112	5.3	5.8
	BB	75	608	44.1	266	8.5	82.6	19.7	28.0
R+A	AN	17	485	45.3	215	5.0	130	4.8	4.2
	BB	37	528	61.2	385	10.4	66.2	14.1	18.0
	ANBB	3	481	77.1	417	4.1	71.3	1.4	1.9
Asia	AN	73	410	32.4	18.4	23.7	12.6	16.2	2.2
	BB	4	475	46.8	441	39.7	73.9	1.1	2.0
NA	AN	132	610	14.2	45.8	1.4	42.4	11.2	8.1
	BB	14	637	10.9	162	1.0	118	1.6	3.5
Source- identified	AN	320	505	24.6	46.6	7.6	44.0	49.2	29.4
	BB	166	576	45.9	272	9.6	73.6	48.7	68.1
	ANBB	5	460	77.1	378	5.6	60.8	2.2	2.6

[a]Median values are shown for these parameters.
[b]APT denotes accumulated precipitation along trajectories.
[c]TE_{BC} and F_A denote transport efficiency of BC defined by equation (1) and fraction of each source to the total amount (sum of the measured concentrations) of species A, which is defined by equation (2), respectively.

Table 3b. Measured and Estimated Statistics of Air Parcels From Individual Sources During the ARCTAS-B (Summer) Campaign

Sources	AN or BB	N	Pressure[a] (hPa)	ΔCO[a] (ppbv)	BC[a] (ng m^{-3})	APT[a,b] (mm)	TE_{BC}[a,c] (%)	$F_{\Delta CO}$[c] (%)	F_{BC}[c] (%)
Russia	AN	8	328	75.3	0.45	37.8	0.18	5.3	1.3
	BB	9	530	50.8	18.4	18.3	4.1	4.4	22.1
	ANBB	10	518	73.7	11.8	27.2	1.6	6.8	10.7
R+A	AN	78	329	78.9	0.99	30.2	0.44	51.2	11.2
	BB	3	523	106	30.5	21.2	3.7	2.4	10.1
	ANBB	13	300	83.8	4.8	51.2	0.74	9.5	12.5
Asia	AN	27	353	59.1	1.4	54.9	0.82	15.6	9.0
	ANBB	2	486	107	9.4	58.8	1.1	1.9	2.0
NA	AN	2	353	54.8	1.5	20.2	0.88	0.97	0.31
	BB	7	330	33.3	23.7	27.9	13.6	1.9	21.1
Source-identified	AN	115	329	77.0	1.1	36.0	0.54	73.0	21.7
	BB	19	523	44.6	22.7	21.2	7.4	8.8	53.2
	ANBB	25	505	83.8	10.0	31.5	1.3	18.2	25.1

[a]Median values are shown for these parameters.
[b]APT denotes accumulated precipitation along trajectories.
[c]TE_{BC} and F_A denote transport efficiency of BC defined by equation (1) and fraction of each source to the total amount (sum of the measured concentrations) of species A, which is defined by equation (2), respectively.

by the concentration of species A at time t from source i ($C_{A,i,t}$), and j means the summation of the concentrations for all sources. The F_{BC} values for AN- and BB-impacted air were 29 and 68%, and those of $F_{\Delta CO}$ were 49 and 49%, respectively (Figure 9 and Table 3a). The F_{BC} and $F_{\Delta CO}$ values for Russian BB air were 28 and 20%. In addition, F_{BC} for BB air parcels that passed over Russia (sum of Russia, Russia+Europe, and Russia+Asia) was as high as 59%, indicating the dominant impact of BC from Russian BB on BC in the North American Arctic. By contrast, the F_{BC} value for Asian AN air was as low as 2.2% (Figure 9 and Tables 3a and 3b), indicating the very limited impact of BC from Asian AN on Arctic BC. Asian AN contributed relatively more to the North American Arctic ΔCO ($F_{\Delta CO}$ was 16%) than BC (F_{BC} was 2%) due to the water insolubility of CO (Table 3a). Other AN sources from Europe, Russia+Europe, Russia, Russia+Asia, and North America each contributed to around 3–10% of BC and ΔCO in the North American Arctic (Table 3a).

3.3. Vertical Profiles

[29] The altitudes of the plumes were also substantially different between the Asian AN and Russian BB air, in addition to the differences in TE_{BC} (Figure 10 and Tables 3a and 3b). Figure 10 shows the vertical profiles of BC and ΔCO. In Figure 10, the median concentrations for all Arctic data during ARCTAS-A are shown together with the median values for each category of air parcel. Since the Asian AN air parcels were transported from lower latitudes (30°–40°N) and experienced WCB rapid ascent, potential temperature increased substantially (high potential temperature at the source and further nonadiabatic heating during transport). Therefore, these air parcels were generally measured in the UT (300–500 hPa). On the other hand, the Russian BB air parcels were transported from higher latitudes (50°–70°N) and experienced near isentropic slow ascent (low potential temperature in the source regions and adiabatic transport). Therefore, the potential temperatures of

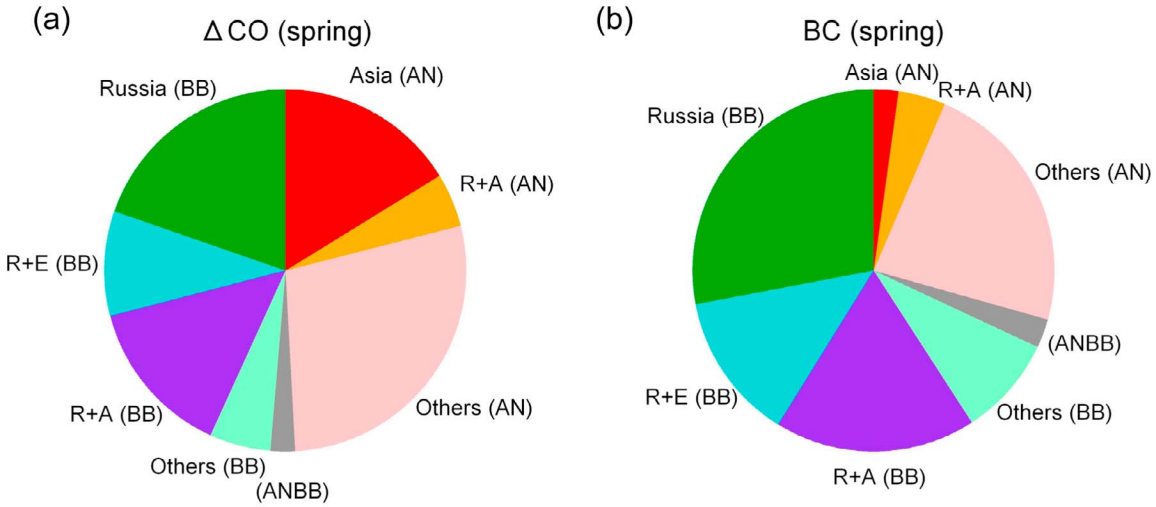

Figure 9. Relative contributions of individual sources to the total amount (sum of the measured concentrations for all source identified air parcels) of (a) ΔCO (F_{CO}) and (b) BC (F_{BC}) during the ARCTAS-A campaign.

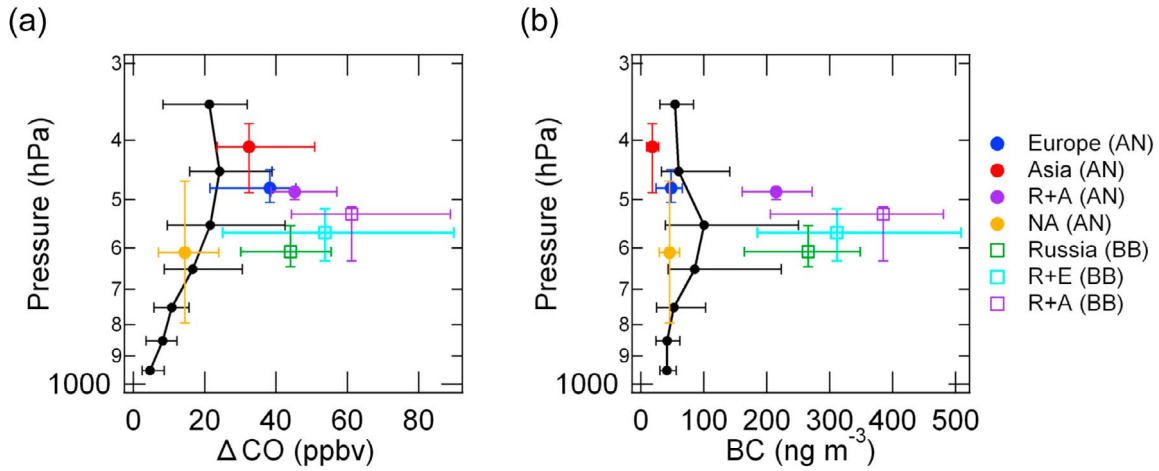

Figure 10. Vertical profiles of (a) ΔCO and (b) BC during the ARCTAS-A campaign. The medians (circles or squares with colors) and 25th to 75th percentiles (horizontal and vertical bars) are shown for individual source regions and fuel types. The black line shows the median vertical profiles for all Arctic data in spring (Flights 6–10).

these air parcels were lower and they were measured in the middle troposphere (MT) (500–700 hPa).

[30] The average ΔCO gradually increased with altitude (Figure 10a), while the BC concentrations showed a broad maximum in the MT (Figure 10b). We can interpret this by the differences in TE_{BC} (section 3.2) and the altitude profiles between the Asian AN and Russian BB air parcels. The increase in ΔCO with altitude was due to the upward transport of the plumes from mid latitudes during their transport to the Arctic in the absence of large sources in the Arctic. The broad peak in BC in the MT was due to the dominant contribution of the BB in Russia. The decrease of BC in the UT was due to wet deposition of BC in Asian AN air. These results will be important in assessing the radiative effects of BC in the Arctic.

4. Seasonal Variation of TE_{BC}

[31] In this section, we present summer (ARCTAS-B) data and compare with the spring (ARCTAS-A) data described in section 3. Figure 11a shows the GPCP mean precipitation distribution before (3–7 July) and during the ARCTAS-B period (8–9 July). A period before the campaign is included considering the transport time from the source regions to the measurement locations. Figures 11b–11d show trajectories of the measured air parcels during ARCTAS-B: AN air from Asia (Asia and Russia+Asia), BB and ANBB air from Russia (Russia and Russia+Asia), and all source-identified data, respectively. The number of source-identified data points in summer is about a factor of 3 smaller than that in spring (Tables 2a and 2b), because the relevant data were obtained only by two flights during ARCTAS-B. The largest portion of air parcels (59%) was classified as Russia+Asia air in summer. Over the latitudes 45°–70°N, precipitation substantially increased in the summertime (Figure 11a) from that in the springtime (Figure 7a). As a result, in summer even the air parcels from Russia and Russia+Asia experienced large APT (>20 mm) (Table 3b). Most air parcels from Asia and Russia+Asia sources experienced WCB transport and were measured in the MT or UT (<600 hPa). Few plumes were sampled in the LT (>600 hPa) during ARCTAS-B.

[32] The difference in the trajectories between spring and summer contributed partly to the seasonal variation of wet removal of Russian and Russia+Asia BB plumes. Some BB air parcels in summer were transported from lower latitudes (<40°N) in East Asia with high relative humidity (Figure 11c). This may have contributed to the increases in the number of ANBB air parcels and lower TE_{BC} in summer. In July, the locations of BB in Siberia shifted slightly northward (to around 50°–60°N) from those in spring [*Jacob et al.*, 2010]. Therefore, TE_{BC} could have been greater in summer if the precipitation distribution had been unchanged. However, the heavier precipitation in summer over the latitudes of 45°–70°N resulted in lower TE_{BC} for Russian BB.

[33] Figure 12 shows the median vertical profiles of BC and ΔCO in spring and summer for all the Arctic data. The median ΔCO concentration was somewhat higher in summer (23 ppbv) than in spring (15 ppbv), although the variabilities (horizontal bars in Figure 12) are generally similar between spring and summer in the mid and upper troposphere (<600 hPa). On the other hand, the median BC concentration was a factor of 10 higher in spring (55 ng m^{-3}) than in summer (5.7 ng m^{-3}), as shown in Figure 12 and Table 4. The median BC/ΔCO ratio was 10–100 times higher in spring (3.8) than in summer (0.042) (Table 4). The large differences in the BC concentration and BC/ΔCO ratio between spring and summer are qualitatively interpreted by the seasonal variation of precipitation over latitudes 45°–70°N, as shown in Figures 7a and 11a. In fact, the median APT of measured air parcels was a factor of 5 larger in summer (17 mm) than in spring (3 mm), as shown in Table 4.

[34] Figure 13 shows correlation plots of the BC/ΔCO ratio and TE_{BC} with APT for Asian AN, Russian BB, Russia+Asia AN, and Russia+Asia BB air in spring and summer. ANBB air parcels in summer were merged into BB air parcels in Figure 13. We assumed that $[BC/\Delta CO]_{source}$ values in summer were the same as those in spring. As shown

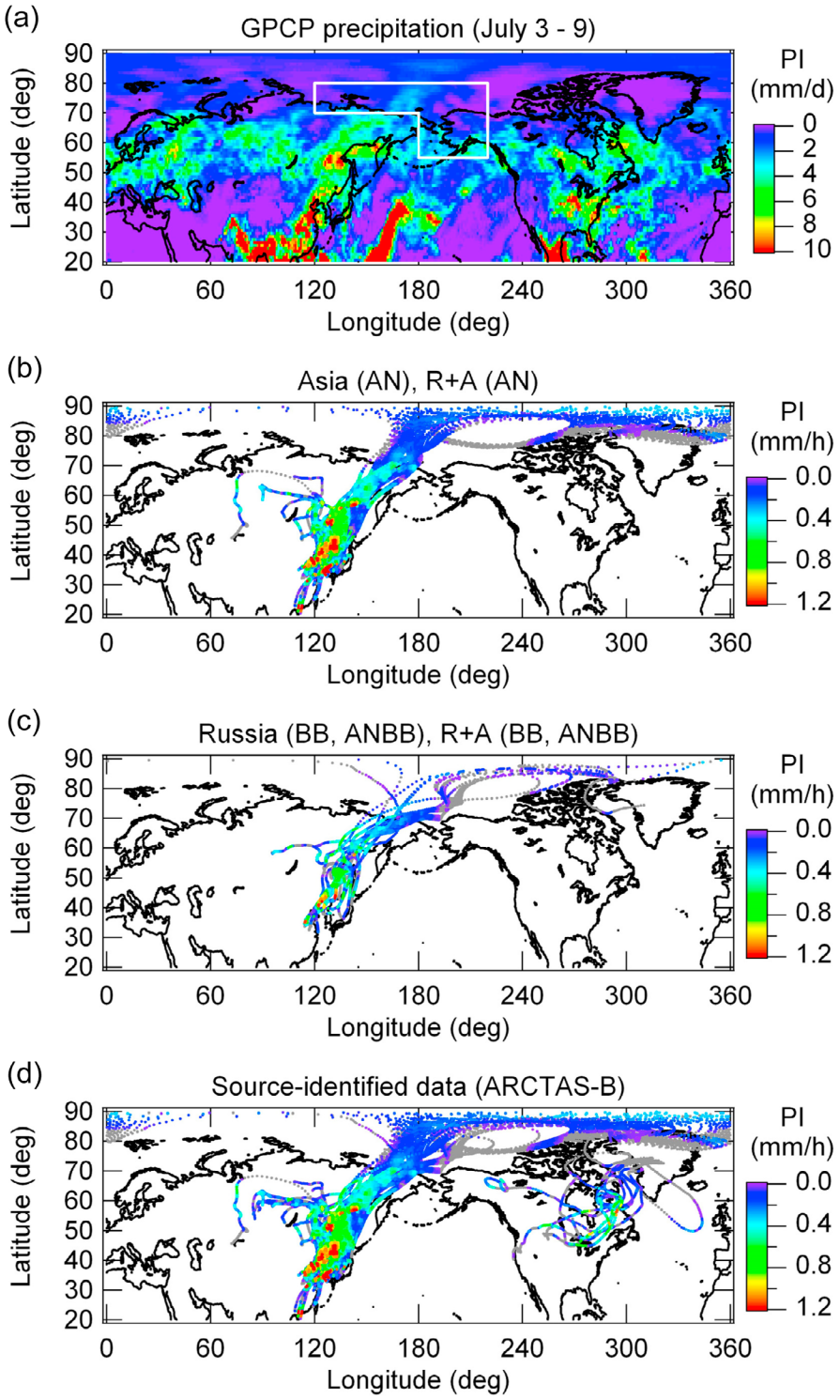

Figure 11. (a) Average precipitation distribution before (3–7 July) and during the ARCTAS-B campaign (8–9 July). A period before the campaign was included considering the transport time from the sources to the measurement locations. The area within the white lines is the Alaskan region defined in section 5. Ten day backward trajectories are shown for (b) air parcels impacted by anthropogenic emissions in Asia (Asia and R+A), (c) air parcels impacted by biomass burning in Russia (Russia, R+E, and R+A), and (d) all the source identified air parcels (see the definition in section 2.3) during the ARCTAS-B campaign. PI denotes precipitation intensity. The periods when PI < 0.01 mm/h are shown with gray dots.

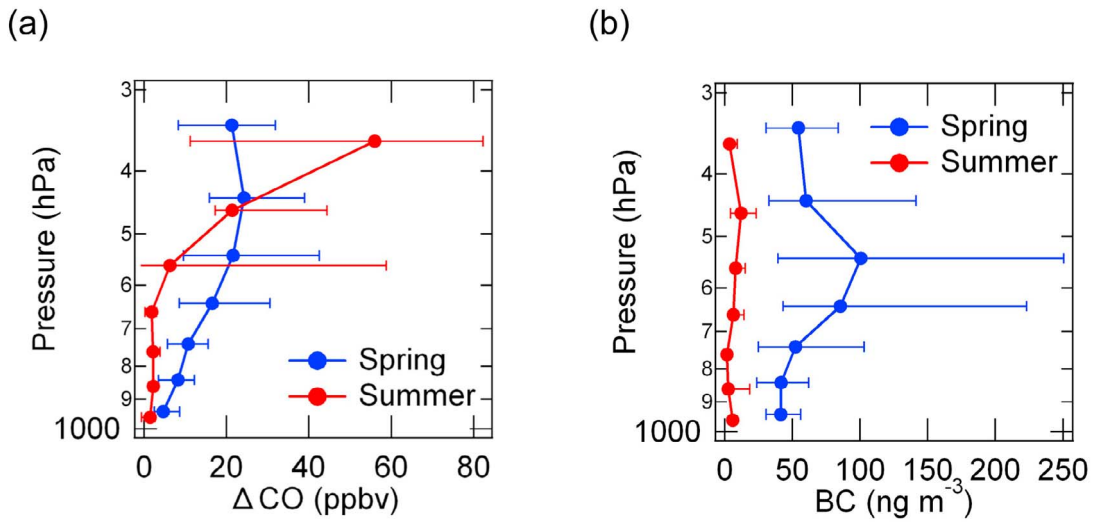

Figure 12. Median vertical profiles of (a) ΔCO and (b) BC for all Arctic data during the ARCTAS-A (blue) and ARCTAS-B (red) campaigns. Horizontal bars show 25th to 75th percentiles at individual altitudes.

in Figure 13b, the TE_{BC} was highly correlated with APT for both seasons. The R^2 values between log (TE_{BC}) and APT in Figure 13b were 1.0 in spring and 0.18 in summer. The lower correlation in summer is mainly due to the lower variability of TE_{BC} than that in spring. While the TE_{BC} from Asian AN plumes were low in both spring (13%) and summer (0.76%), those from Russian BB plumes showed a large difference between spring (87%) and summer (4.0%). These results demonstrate that Russian BB emissions in spring were more important and more efficiently transported BC to the Arctic than those in summer.

5. ARCTAS Data Viewed in the Longer-Term Record of Aerosol Data

[35] In this section, we examine the degree of deviation of the aerosol concentrations in the measured air parcels during the ARCTAS campaign using satellite measurements from the Moderate Resolution Imaging Spectroradiometer (MODIS) [*Remer et al.*, 2005] and Measurements of Pollution in the Troposphere (MOPITT) instrument [*Drummond and Mand*, 1996; *Bowman*, 2006]. MODIS Level 3 daily global products (resolution of 1 × 1 degree) on both the Terra (MOD08_D3) and Aqua (MYD08_D03) satellites were used for column AOD. We used the average of the two satellite data sets unless one of them was unavailable. MOPITT Level 3 daily average global data (resolution of 1 × 1 degree) on the Terra satellite were used for column CO concentration. Daytime data were used in this study.

[36] Figure 14 shows the median column CO concentrations and AOD values over the Alaskan region within 1 month periods in April and July for the years from 2002 to 2009. The values during the ARCTAS campaign and the 2002–2009 period are also shown in Figure 14 in the "ARCTAS" and "2002–2009" columns, respectively. The Alaskan region was defined as the area within the white lines shown in Figure 11a and was used because of the major measurement regions or transport pathways of air parcels during the ARCTAS campaign. The amount of available MODIS data is very limited in April, because a large part of the Alaskan region is covered by snow/ice surface (high albedo) in this season. Monthly fire counts (using global fire count data from MODIS, MOD14CM1) north of 50°N are also shown in Figure 14 for the same periods. AOD represents the total aerosol concentrations in the column rather than the BC concentrations focused on in this study. However, the column AODs represent BC mass concentrations in the column as well, considering that the volume concentrations of scattering aerosols measured by the SP2 instrument were highly correlated with BC mass concentrations, with $R^2 = 0.86$ for spring and 0.74 for summer.

[37] The "ARCTAS" and "2008" CO and AOD column data show that the values during ARCTAS-A and ARCTAS-B were similar to the monthly averages (April and July 2008). On the other hand, the column CO and AOD in April 2008 were greater than those in the other years. When we compared the "2008" and "2002–2009" columns, the median CO, ΔCO (when a background concentration of 2.4×10^{18} molecules cm^{-2} was assumed), and AOD in April 2008 were 1.0, 1.7,

Table 4. Statistics of All Measured Air Parcels During the ARCTAS Campaign[a]

Season	N	Pressure[b] (hPa)	ΔCO[b] (ppbv)	BC[b] (ng m^{-3})	BC/ΔCO[b]	APT[b,c] (mm)
Spring (ARCTAS-A)	1954	606 (*553*)	20.9 (*13.8*)	107 (*55.0*)	4.3 (*3.8*)	6.8 (*3.2*)
Summer (ARCTAS-B)	447	432 (*365*)	35.7 (*23.0*)	9.9 (*5.7*)	0.29 (*0.042*)	20.8 (*16.7*)

[a]These statistics are calculated for all Arctic data (blue and red lines in Figure 1).
[b]Average and median (italics within parentheses) values are shown for these parameters.
[c]APT denotes accumulated precipitation along trajectories.

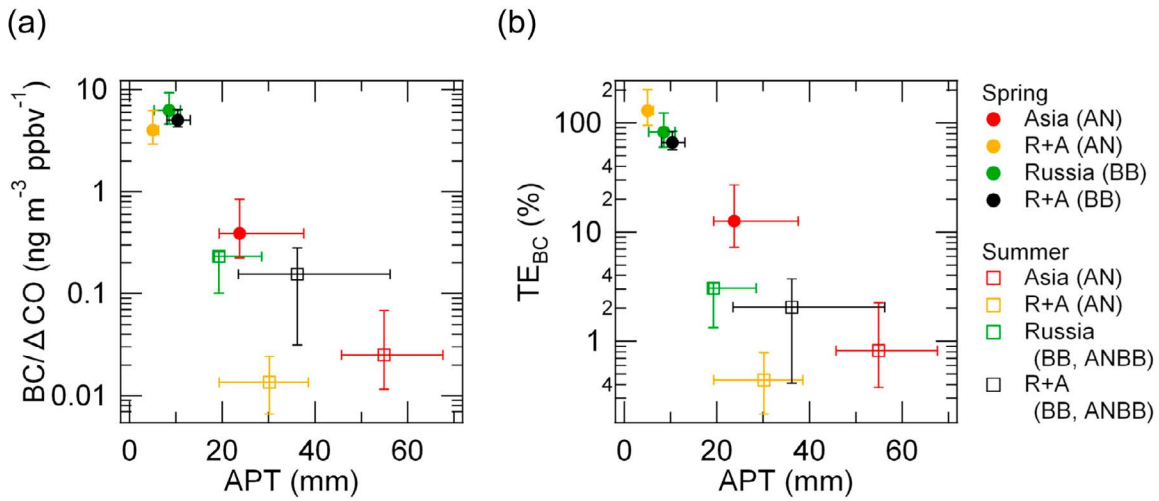

Figure 13. Scatterplots of (a) BC/ΔCO ratio and (b) transport efficiency of BC (TE_{BC}) as a function of APT. The medians (circles or squares) and 25th to 75th percentiles (horizontal and vertical bars) are shown for the individual source regions and fuel types during the ARCTAS-A (solid circles) and ARCTAS-B (open squares) campaigns.

and 1.5 times higher than those in April for the 2002–2009 period. The main cause is that Russian BB started unusually early in spring in 2008, consistent with the higher fire counts by a factor of 2.3 in April 2008 than those for the 2002–2009 period. The variability (vertical bars in Figure 14) of CO is similar or larger in summer than in spring (2.7×10^{17} molecules cm^{-2} in spring and 4.0×10^{17} molecules cm^{-2} in summer for the 2002–2009 period), while that of AOD is larger in spring than in summer, except for the years 2004 and 2009, when intense fires occurred in Alaska in summer (0.13 in spring for the 2002–2009 period and 0.092 in summer for the 2002–2003 and 2005–2008 periods). This

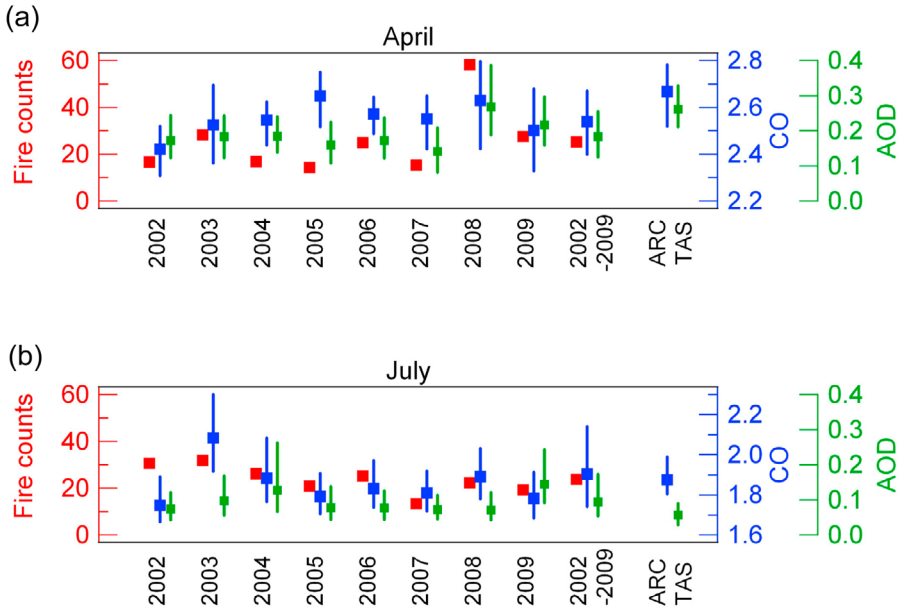

Figure 14. Column CO (blue, right axis, MOPITT) and AOD (green, right axis, MODIS) over the Alaskan region (defined as area within white lines in Figure 11a) in (a) April and (b) July. The medians (squares) and 25th to 75th percentiles (vertical bars) for the 1 month periods are shown from year 2002 to 2009. The medians and 25th to 75th percentiles during the ARCTAS period and the 2002–2009 period are shown in columns marked "ARCTAS" and "2002–2009," respectively. Monthly fire counts (red, left axis, MODIS) north of 50°N are also shown. The units of the column CO, column AOD, and fire counts are molecules cm^{-2} ($\times 10^{18}$), dimensionless, and numbers ($\times 1000$), respectively.

result is consistent with lower variability in BC (and aerosols) in summer due to a higher degree of wet removal. The ratios of median CO, ΔCO (when a background concentration of 1.7×10^{18} molecules cm^{-2} was assumed), AOD, and fire counts in July 2008 to the 2002–2009 period were 0.99, 0.93, 0.75, and 0.94, respectively.

[38] Meteorological conditions are also important to understand year-to-year variations of aerosol transport to the Arctic more precisely. Recent studies suggest that year-to-year variations of the transport of pollutants from the mid latitudes to the Arctic are largely dependent on meteorological oscillation phenomena, such as the North Atlantic Oscillation (NAO) [*Eckhardt et al.*, 2003; *Duncan and Bey*, 2004; *Burkhart et al.*, 2006; *Fuelberg et al.*, 2010] and the El Niño Southern Oscillation (ENSO) [*Fisher et al.*, 2010]. Both the NAO Index (NAOI) and Ocean Niño Index (ONI) were negative during the ARCTAS-A campaign. The negative NAOI (lower meridional gradient of sea level pressure over the north Atlantic) means weaker winds over Europe and reduces the export of pollution to the Arctic [*Duncan and Bey*, 2004]. The negative ONI (La Niña) means a weaker Aleutian low, which decreases the northward transport of pollutants from Asia to the Alaskan region [*Fisher et al.*, 2010; *Niebauer*, 1988].

[39] Based on these indices, the transport from mid latitudes to the Arctic is considered to have been weaker in 2008 than usual [*Fuelberg et al.*, 2010; *Fisher et al.*, 2010]. In fact, despite the anomalously large Russian BB in April 2008 (fire counts were 2.3 times higher in April 2008 than the 2002–2009 period), the column ΔCO and AOD over the Alaskan region in 2008 were higher by only 1.7 and 1.5 times, respectively, than the average values for the 2002–2009 period. This result is qualitatively consistent with the negative ONI in 2008 and previous studies [*Fisher et al.*, 2010]. Further detailed studies considering meteorological conditions are needed to understand year-to-year variations of aerosols in the Arctic more quantitatively.

6. Summary and Conclusion

[40] We have quantified the pathways and efficiencies of BC transport from different regions and fuel types of combustion (anthropogenic (AN) and biomass burning (BB)) to the Arctic region using data obtained by the ARCTAS aircraft campaign conducted in April and June–July 2008. We focused on AN air parcels transported from East Asia (Asian AN) and BB air parcels from Russia (Russian BB). The source regions and fuel types were identified by backward trajectory calculations and hydrocarbon tracers, respectively. The BC transport efficiency (TE_{BC}) was interpreted in relation to the accumulated precipitation along the trajectories (APT).

[41] In the springtime, the median BC concentrations (18 ng m^{-3}) and TE_{BC} (13%) in Asian AN air were much lower than those in Russian BB air (266 ng m^{-3} and 83%, respectively). The lower BC values in Asian AN air were due to more efficient wet deposition, represented by the larger APT of 24 mm versus 8.5 mm for Russian BB air. Most Asian AN air parcels were transported from lower latitudes (30°–40°N) with high relative humidity and experienced rapid ascent by warm conveyor belts (WCBs) with heavy precipitation. On the other hand, Russian BB air parcels were transported almost isentropically with low precipitation from higher latitudes (50°–70°N) with low relative humidity.

[42] The altitude distributions of BC and ΔCO were substantially different between Asian AN and Russian BB air. The Asian AN air parcels were typically measured in the upper troposphere (UT) and the Russian BB air parcels in the middle troposphere (MT). The median BC concentrations reached a maximum in the MT, while ΔCO remained high in the UT, uninfluenced by wet deposition.

[43] The contribution of BB air from Russia to BC in the North American Arctic (F_{BC}) was dominant (59%), and that of Asian AN air was only about 2%. The contributions of these sources to ΔCO were more comparable, i.e., 43% versus 16%, which were controlled by emissions and transport uninfluenced by wet deposition. No air parcels from south Asian sources (<30°N) reached the Arctic, leading to little contribution to BC in the North American Arctic during the ARCTAS-A campaign.

[44] In summer, the median BC mass concentrations for all air parcels was 5.7 ng m^{-3}, which is 10 times lower than those in spring (55 ng m^{-3}), while the median ΔCO mixing ratio was somewhat higher than that in spring (23 ppbv versus 14 ppbv). The TE_{BC} values for both Russian BB and Asian AN air were much lower in summer (4.0 and 0.76%, respectively) than those in spring (83 and 13%, respectively). Correspondingly, the median APT in summer was much higher (17 mm) than that in spring (3.2 mm) for all Arctic air parcels. This is mainly due to the higher precipitation over the latitudes of 45°–70°N in summer. The TE_{BC}-APT correlation, together with the seasonal variations in APT, shows that the large seasonal variations in BC were caused mainly by those in the wet removal rates. The contribution of Russian BB in spring to North American Arctic BC concentrations was largest, because of the spring maximum in TE_{BC} with low precipitation at higher latitudes.

[45] BB in Russia may increase in the future due to global warming [e.g., *Stocks et al.*, 1998]. The possible earlier onset of Russian BB could accelerate warming in the Arctic through the snow-albedo feedback and longwave indirect effect. The high efficiency of BC transport emitted from Russian BB indicates this source has a large and realistic potential for this feedback to be effective, leading to acceleration of the warming of the Arctic in the future.

Appendix A

A1. Uncertainties in Trajectory Calculations

[46] In this section, we evaluate the uncertainties in the identification of source regions discussed in section 2.2 from the comparison of two kinematic backward trajectory calculations (TRJ1 and TRJ2). For this paper, we used TRJ1 trajectories, calculated by using the model of *Fuelberg et al.* [2010] with meteorological data from the WRF model. TRJ2 trajectories were calculated by using the NIPR trajectory model [*Tomikawa and Sato*, 2005] combined with NCEP-FNL meteorological data. The horizontal (45 × 45 km), vertical (50 layers), and temporal (1 h) resolutions of the WRF model results are higher than those (1 × 1 degree, 26 layers, and 6 h) of NCEP-FNL objective analysis data. The identified source regions can be different depending on the differences in the trajectories, TRJ1 and TRJ2. As a result, statistics for each source region, including the data

Table A1. Classification and Statistical Results Using Two Different Trajectory Calculations During the ARCTAS-A (Spring) Campaign

Sources	AN or BB	Trajectory[a]	N	Pressure[b]	ΔCO[b] (ppbv)	BC[b] (ng m^{-3})	APT[b,c] (mm)	TE_{BC}[b,d] (%)
R+E	AN	TRJ1	33	489	34.4	104	11.0	110
		TRJ2	52	500	34.1	77.7	10.6	70.8
	BB	TRJ1	29	566	53.8	312	11.6	74.3
		TRJ2	26	544	54.5	266	10.0	62.9
Russia	AN	TRJ1	38	614	22.2	96.4	5.5	112
		TRJ2	48	529	24.8	99.4	4.3	115
	BB	TRJ1	75	608	44.1	266	8.5	82.6
		TRJ2	87	595	41.0	253	9.3	81.8
R+A	AN	TRJ1	17	485	45.3	215	5.0	130
		TRJ2	45	466	38.1	190	6.5	137
	BB	TRJ1	37	528	61.2	385	10.4	66.2
		TRJ2	46	530	49.5	259	9.7	74.5
Asia	AN	TRJ1	73	410	32.4	18.4	23.7	12.6
		TRJ2	84	410	32.9	21.6	26.8	13.5

[a]TRJ1 is a kinematic trajectory calculation using meteorological input from the WRF model [*Fuelberg et al.*, 2010]. TRJ2 is a kinematic trajectory calculation using NIPR trajectory model [*Tomikawa and Sato*, 2005] and meteorological input of NCEP-FNL data.
[b]Median values are shown for these parameters.
[c]APT denotes accumulated precipitation along trajectories.
[d]TE_{BC} denotes transport efficiency of BC defined by equation (1).

point number, measured pressure, ΔCO, and BC, accumulated precipitation along trajectories (APT), and TE_{BC} can also be different for the same measurement data on board the DC-8.

[47] Table A1 shows the classification and statistical results of TRJ1 and TRJ2 calculations during the ARCTAS-A campaign. The Russian and Asian air parcels (Russia+Europe, Russia, Russia+Asia, and Asia) are shown because we focused on them in this study. We used the same analysis methods and measurement data in this estimation, and the statistical differences between TRJ1 and TRJ2 were caused solely by the differences in the trajectory calculations. The APT values were calculated using GPCP global precipitation data by the method shown in section 2.2. Common features are found in the median values of the parameters for the different types of air parcels, identified using the TRJ1 and TRJ2 trajectories, as summarized in Table A1. The number of data points is greater for the Asian AN and Russian BB air parcels (73–87) than the Russia+Europe and Russia+Asia air parcels (17–52). The measured pressure for the Asian AN air (410 hPa) is lower than that of the Russian AN and BB air (529–614 hPa). The median values of BC (253–385 ng m^{-3}) and TE_{BC} (63–83%) for the Russia+Europe BB, Russian BB, and Russia+Asia BB air were much higher than the values of BC (18–22 ng m^{-3}) and TE_{BC} (13–14%) for the Asian AN air, corresponding to the systematic difference in the APT values. These results show that the median values of the key parameters and the conclusions drawn from them do not depend on the choice of the calculation methods or meteorological inputs used for the TRJ1 and TRJ2 trajectories.

A2. Uncertainties in the APT

[48] In order to evaluate the uncertainties in the estimation of APT, we compared the APT values calculated using three different precipitation data sets: (1) GPCP global precipitation data, which are mainly used in this study, with horizontal and temporal resolutions of 1 × 1 degree and 1 day; (2) CMAP global precipitation data, with horizontal and temporal resolutions of 2.5 × 2.5 degrees and 5 days; and (3) WRF model calculations, with horizontal and temporal resolutions of 45 × 45 km and 1 h. The methodologies used in constructing the three data sets are quite different, as are their horizontal and temporal resolutions. The GPCP and CMAP data are based on gauge measurements and satellite estimates of rainfall. The GPCP data were derived only from measurements, while the CMAP data were estimated using both measurements and precipitation forecasts from the NCEP-NCAR reanalysis. The GPCP and CMAP data have coarser resolutions than those of the WRF data, which are based on model calculations.

[49] The APT values were calculated using the three precipitation data sets by the method shown in section 2.2. The results from TRJ1 [*Fuelberg et al.*, 2010] were used in this calculation. Table A2 shows the median APT values for three precipitation data sets during the ARCTAS-A campaign. As shown in Table A2, the difference in APT between the three precipitation data sets is quite small. For example, median APT for the Asian AN air is the highest (within 23–25 mm), while those for the Russian AN (4–6 mm) and BB (5–8 mm) air are very low for all three data sets. In addition, the temporal variations of the APT data sets agreed reasonably well for the ARCTAS-A campaign period: the correlation coefficient (R^2) was 0.71 between GPCP and CMAP data and 0.36 between GPCP and WRF data for the Arctic data. These results show that the APT values are insensitive

Table A2. Medians of Accumulated Precipitation Along Trajectories Using Three Different Data Sets of Precipitation During the ARCTAS-A (Spring) Campaign

Source	AN or BB	GPCP (mm)	CMAP (mm)	WRF (mm)
R+E	AN	11.0	8.1	11.8
	BB	11.6	9.3	9.4
Russia	AN	5.5	5.5	4.5
	BB	8.5	6.1	7.9
R+A	AN	5.0	5.6	7.7
	BB	10.4	6.5	7.6
Asia	AN	23.7	24.7	23.2
Source-identified	—	8.7	6.9	7.6
Arctic data	—	3.2	5.3	3.8

to the choice of precipitation data set for the horizontal and temporal scales adopted for this study. We conclude that APT is a reliable measure to represent the amount of precipitation that air parcels experienced during transport.

[50] **Acknowledgments.** The ARCTAS campaign was supported by NASA. We are indebted to all the ARCTAS participants for their cooperation and support. Special thanks are due to the flight and ground crews of the NASA DC-8 aircraft. We thank M. Osuka for his assistance with the field measurements. This work was supported in part by the Ministry of Education, Culture, Sports, Science, and Technology (MEXT), the strategic international cooperative program of the Japan Science and Technology Agency (JST), and the global environment research fund of the Japanese Ministry of the Environment (B-083). Y.Z. was supported in part by NASA Tropospheric Chemistry Program (USP-SMD-08-009). CH_3CN measurements were supported by the Austrian Research Promotion Agency (FFG-ALR) and the Tiroler Zukunftstiftung and carried out with the help/support of T. Mikoviny, M. Graus, A. Hansel, and T. D. Maerk.

References

Adler, R. F., et al. (2003), The Version 2 Global Precipitation Climatology Project (GPCP) monthly precipitation analysis (1979–Present), *J. Hydrometeorol.*, *4*, 1147–1167, doi:10.1175/1525-7541(2003)004<1147:TVGPCP>2.0.CO;2.

Barrie, L. A. (1986), Arctic air pollution: An overview of current knowledge, *Atmos. Environ.*, *20*, 643–663, doi:10.1016/0004-6981(86)90180-0.

Baumgardner, D., G. Kok, and G. Raga (2004), Warming of the Arctic lower stratosphere by light absorbing particles, *Geophys. Res. Lett.*, *31*, L06117, doi:10.1029/2003GL018883.

Blake, N. J., et al. (2003), NMHCs and halocarbons in Asian continental outflow during the Transport and Chemical Evolution over the Pacific (TRACE-P) Field Campaign: Comparison with PEM-West B, *J. Geophys. Res.*, *108*(D20), 8806, doi:10.1029/2002JD003367.

Bowman, K. P. (2006), Transport of carbon monoxide from the tropics to the extratropics, *J. Geophys. Res.*, *111*, D02107, doi:10.1029/2005JD006137.

Burkhart, J. F., R. C. Bales, J. R. McConnell, and M. A. Hutterli (2006), Influence of North Atlantic Oscillation on anthropogenic transport recorded in northwest Greenland ice cores, *J. Geophys. Res.*, *111*, D22309, doi:10.1029/2005JD006771.

Chen, M., R. Talbot, H. Mao, B. Sive, J. Chen, and R. J. Griffin (2007), Air mass classification in coastal New England and its relationship to meteorological conditions, *J. Geophys. Res.*, *112*, D10S05, doi:10.1029/2006JD007687.

Choi, Y., S. Elliott, I. J. Simpson, D. R. Blake, J. J. Colman, M. K. Dubey, S. Meinardi, F. S. Rowland, T. Shirai, and F. A. Smith (2003), Survey of whole air data from the second airborne Biomass Burning and Lightning Experiment using principal component analysis, *J. Geophys. Res.*, *108*(D5), 4163, doi:10.1029/2002JD002841.

Clarke, A. D., and K. J. Noone (1985), Soot in the Arctic snowpack: A cause for perturbations in radiative transfer, *Atmos. Environ.*, *19*(12), 2045–2053, doi:10.1016/0004-6981(85)90113-1.

de Gouw, J. A., et al. (2004), Chemical composition of air masses transported from Asia to the U.S. West Coast during ITCT 2K2: Fossil fuel combustion versus biomass-burning signatures, *J. Geophys. Res.*, *109*, D23S20, doi:10.1029/2003JD004202.

Drummond, J. R., and G. S. Mand (1996), The Measurements of Pollution in the Troposphere (MOPITT) Instrument: Overall performance and calibration requirements, *J. Atmos. Oceanic Technol.*, *13*, 314–320, doi:10.1175/1520-0426(1996)013<0314:TMOPIT>2.0.CO;2.

Duncan, B. N., and I. Bey (2004), A modeling study of the export pathways of pollution from Europe: Seasonal and interannual variations (1987–1997), *J. Geophys. Res.*, *109*, D08301, doi:10.1029/2003JD004079.

Eck, T. F., et al. (2009), Optical properties of boreal region biomass burning aerosols in central Alaska and seasonal variation of aerosol optical depth at an Arctic coastal site, *J. Geophys. Res.*, *114*, D11201, doi:10.1029/2008JD010870.

Eckhardt, S., A. Stohl, S. Beirle, N. Spichtinger, P. James, C. Forster, C. Junker, T. Wagner, U. Platt, and S. G. Jennings (2003), The North Atlantic Oscillation controls air pollution transport to the Arctic, *Atmos. Chem. Phys.*, *3*(5), 1769–1778, doi:10.5194/acp-3-1769-2003.

Eleftheriadis, K., S. Vratolis, and S. Nyeki (2009), Aerosol black carbon in the European Arctic: Measurements at Zeppelin station, Ny-Ålesund, Svalbard from 1998–2007, *Geophys. Res. Lett.*, *36*, L02809, doi:10.1029/2008GL035741.

Engvall, A., J. Ström, P. Tunved, R. Krejci, H. Schlager, and A. Minikin (2009), The radiative effect of an aged, internally mixed Arctic aerosol originating from lower-latitude biomass burning, *Tellus, Ser. B*, *61*(4), 677–684, doi:10.1111/j.1600-0889.2009.00431.x.

Fisher, J. A., et al. (2010), Source attribution and interannual variability of Arctic pollution in spring constrained by aircraft (ARCTAS, ARCPAC) and satellite (AIRS) observations of carbon monoxide, *Atmos. Chem. Phys.*, *10*(3), 977–996, doi:10.5194/acp-10-977-2010.

Flanner, M. G., C. S. Zender, J. T. Randerson, and P. J. Rasch (2007), Present-day climate forcing and response from black carbon in snow, *J. Geophys. Res.*, *112*, D11202, doi:10.1029/2006JD008003.

Flanner, M. G., C. S. Zender, P. G. Hess, N. M. Mahowald, T. H. Painter, V. Ramanathan, and P. J. Rasch (2009), Springtime warming and reduced snow cover from carbonaceous particles, *Atmos. Chem. Phys.*, *9*(7), 2481–2497, doi:10.5194/acp-9-2481-2009.

Fuelberg, H. E., D. L. Harrigan, and W. Sessions (2010), A meteorological overview of the ARCTAS 2008 mission, *Atmos. Chem. Phys.*, *10*(2), 817–842, doi:10.5194/acp-10-817-2010.

Garrett, T. J., and C. Zhao (2006), Increased Arctic cloud longwave emissivity associated with pollution from mid-latitudes, *Nature*, *440*(7085), 787–789, doi:10.1038/nature04636.

Garrett, T. J., C. Zhao, and P. C. Novelli (2010), Assessing the relative contributions of transport efficiency and scavenging to seasonal variability in Arctic aerosol, *Tellus, Ser. B*, *62*, 190–196, doi:10.1111/j.1600-0889.2010.00453.x.

Gong, S. L., T. L. Zhao, S. Sharma, D. Toom-Sauntry, D. Lavoué, X. B. Zhang, W. R. Leaitch, and L. A. Barrie (2010), Identification of trends and interannual variability of sulfate and black carbon in the Canadian High Arctic: 1981–2007, *J. Geophys. Res.*, *115*, D07305, doi:10.1029/2009JD012943.

Han, S., et al. (2009), Temporal variations of elemental carbon in Beijing, *J. Geophys. Res.*, *114*, D23202, doi:10.1029/2009JD012027.

Hansen, J., and L. Nazarenko (2004), Soot climate forcing via snow and ice albedos, *Proc. Natl. Acad. Sci. U. S. A.*, *101*(2), 423–428, doi:10.1073/pnas.2237157100.

Hsu, N. C., J. R. Herman, J. F. Gleason, O. Torres, and C. J. Seftor (1999), Satellite detection of smoke aerosols over a snow/ice surface by TOMS, *Geophys. Res. Lett.*, *26*(8), 1165–1168, doi:10.1029/1999GL900155.

Huang, L., S. L. Gong, S. Sharma, D. Lavoué, and C. Q. Jia (2010), A trajectory analysis of atmospheric transport of black carbon aerosols to Canadian high Arctic in winter and spring (1990–2005), *Atmos. Chem. Phys.*, *10*(11), 5065–5073, doi:10.5194/acp-10-5065-2010.

Huffman, G. J., R. F. Adler, M. M. Morrissey, D. T. Bolvin, S. Curtis, R. Joyce, B. McGavock, and J. Susskind (2001), Global precipitation at one-degree daily resolution from multisatellite observations, *J. Hydrometeorol.*, *2*, 36–50, doi:10.1175/1525-7541(2001)002<0036:GPAODD>2.0.CO;2.

Iziomon, M. G., U. Lohmann, and P. K. Quinn (2006), Summertime pollution events in the Arctic and potential implications, *J. Geophys. Res.*, *111*, D12206, doi:10.1029/2005JD006223.

Jacob, D. J., et al. (2010), The Arctic Research of the Composition of the Troposphere from Aircraft and Satellites (ARCTAS) mission: Design, execution, and first results, *Atmos. Chem. Phys.*, *10*(11), 5191–5212, doi:10.5194/acp-10-5191-2010.

Kim, Y., H. Hatsushika, R. R. Muskett, and K. Yamazaki (2005), Possible effect of boreal wildfire soot on Arctic sea ice and Alaska glaciers, *Atmos. Environ.*, *39*(19), 3513–3520, doi:10.1016/j.atmosenv.2005.02.050.

Klonecki, A., P. Hess, L. Emmons, L. Smith, J. Orlando, and D. Blake (2003), Seasonal changes in the transport of pollutants into the Arctic troposphere-model study, *J. Geophys. Res.*, *108*(D4), 8367, doi:10.1029/2002JD002199.

Koch, D., and J. Hansen (2005), Distant origins of Arctic black carbon: A Goddard Institute for Space Studies ModelE experiment, *J. Geophys. Res.*, *110*, D04204, doi:10.1029/2004JD005296.

Koike, M., et al. (2003), Export of anthropogenic reactive nitrogen and sulfur compounds from the East Asia region in spring, *J. Geophys. Res.*, *108*(D20), 8789, doi:10.1029/2002JD003284.

Kondo, Y., L. Sahu, N. Moteki, F. Khan, N. Takegawa, X. Liu, M. Koike, and T. Miyakawa (2011a), Consistency and traceability of black carbon measurements made by laser-induced incandescence, thermal-optical transmittance, and filter-based photo-absorption techniques, *Aerosol Sci. Technol.*, *45*(2), 295–312.

Kondo, Y., et al. (2011b), Emissions of black carbon, organic, and inorganic aerosols from biomass burning in North America and Asia in 2008, *J. Geophys. Res.*, doi:10.1029/2010JD015152, in press.

Law, K. S., and A. Stohl (2007), Arctic air pollution: Origins and impacts, *Science*, *315*(5818), 1537–1540, doi:10.1126/science.1137695.

Lubin, D., and A. M. Vogelmann (2006), A climatologically significant aerosol longwave indirect effect in the Arctic, *Nature*, *439*(7075), 453–456, doi:10.1038/nature04449.

Matsui, H., et al. (2009), Spatial and temporal variations of aerosols around Beijing in summer 2006: Model evaluation and source apportionment, *J. Geophys. Res.*, *114*, D00G13, doi:10.1029/2008JD010906.

Moteki, N., and Y. Kondo (2007), Effects of mixing state on black carbon measurements by laser-induced incandescence, *Aerosol Sci. Technol.*, *41*(4), 398–417, doi:10.1080/02786820701199728.

Moteki, N., and Y. Kondo (2010), Dependence of laser-induced incandescence on physical properties of black carbon aerosols: Measurements and theoretical interpretation, *Aerosol Sci. Technol.*, *44*(8), 663–675, doi:10.1080/02786826.2010.484450.

Niebauer, H. J. (1988), Effects of El Nino-Southern Oscillation and North Pacific weather patterns on interannual variability in the subarctic Bering Sea, *J. Geophys. Res.*, *93*(C5), 5051–5068, doi:10.1029/JC093iC05p05051.

Oshima, N., et al. (2004), Asian chemical outflow to the Pacific in late spring observed during the PEACE-B aircraft mission, *J. Geophys. Res.*, *109*, D23S05, doi:10.1029/2004JD004976.

Paris, J., A. Stohl, P. Nédélec, M. Y. Arshinov, M. V. Panchenko, V. P. Shmargunov, K. S. Law, B. D. Belan, and P. Ciais (2009), Wildfire smoke in the Siberian Arctic in summer: Source characterization and plume evolution from airborne measurements, *Atmos. Chem. Phys.*, *9*(23), 9315–9327, doi:10.5194/acp-9-9315-2009.

Park, R. J., et al. (2005), Export efficiency of black carbon aerosol in continental outflow: Global implications, *J. Geophys. Res.*, *110*, D11205, doi:10.1029/2004JD005432.

Polissar, A. V., P. K. Hopke, P. Paatero, Y. J. Kaufmann, D. K. Hall, B. A. Bodhaine, E. G. Dutton, and J. M. Harris (1999), The aerosol at Barrow, Alaska: Long-term trends and source locations, *Atmos. Environ.*, *33*(16), 2441–2458, doi:10.1016/S1352-2310(98)00423-3.

Quinn, P. K., T. L. Miller, T. S. Bates, J. A. Ogren, E. Andrews, and G. E. Shaw (2002), A 3-year record of simultaneously measured aerosol chemical and optical properties at Barrow, Alaska, *J. Geophys. Res.*, *107*(D11), 4130, doi:10.1029/2001JD001248.

Quinn, P. K., G. Shaw, E. Andrews, E. G. Dutton, T. Ruoho-Airola, and S. L. Gong (2007), Arctic haze: Current trends and knowledge gaps, *Tellus, Ser. B*, *59*(1), 99–114, doi:10.1111/j.1600-0889.2006.00238.x.

Quinn, P. K., et al. (2008), Short-lived pollutants in the Arctic: Their climate impact and possible mitigation strategies, *Atmos. Chem. Phys.*, *8*(6), 1723–1735, doi:10.5194/acp-8-1723-2008.

Remer, L. A., et al. (2005), The MODIS aerosol algorithm, products, and validation, *J. Atmos. Sci.*, *62*, 947–973, doi:10.1175/JAS3385.1.

Sachse, G. W., G. F. Hill, L. O. Wade, and M. G. Perry (1987), Fast-response, high precision carbon monoxide sensor using a tunable diode laser absorption technique, *J. Geophys. Res.*, *92*, 2071–2081.

Sharma, S., J. R. Brook, H. Cachier, J. Chow, A. Gaudenzi, and G. Lu (2002), Light absorption and thermal measurements of black carbon in different regions of Canada, *J. Geophys. Res.*, *107*(D24), 4771, doi:10.1029/2002JD002496.

Sharma, S., D. Lavoue, H. Cachier, L. A. Barrie, and S. L. Gong (2004), Long-term trends of the black carbon concentrations in the Canadian Arctic, *J. Geophys. Res.*, *109*, D15203, doi:10.1029/2003JD004331.

Sharma, S., E. Andrews, L. A. Barrie, J. A. Ogren, and D. Lavoué (2006), Variations and sources of the equivalent black carbon in the high Arctic revealed by long-term observations at Alert and Barrow: 1989–2003, *J. Geophys. Res.*, *111*, D14208, doi:10.1029/2005JD006581.

Shaw, G. E. (1995), The Arctic haze phenomenon, *Bull. Am. Meteorol. Soc.*, *76*(12), 2403–2413, doi:10.1175/1520-0477(1995)076<2403:TAHP>2.0.CO;2.

Shindell, D., and G. Faluvegi (2009), Climate response to regional radiative forcing during the twentieth century, *Nat. Geosci.*, *2*(4), 294–300, doi:10.1038/ngeo473.

Shindell, D. T., et al. (2008), A multi-model assessment of pollution transport to the Arctic, *Atmos. Chem. Phys.*, *8*(17), 5353–5372, doi:10.5194/acp-8-5353-2008.

Shipham, M. C., A. S. Bachmeier, D. R. C. Jr., and E. V. Browell (1992), Meteorological overview of the Arctic Boundary Layer Expedition (ABLE 3A) flight series, *J. Geophys. Res.*, *97*(D15), 16,395–16,419.

Sirois, A., and L. A. Barrie (1999), Arctic lower tropospheric aerosol trends and composition at Alert, Canada: 1980–1995, *J. Geophys. Res.*, *104*(D9), 11,599–11,618, doi:10.1029/1999JD900077.

Skamarock, W. C., J. B. Klemp, J. Dudhia, D. O. Gill, D. M. Barker, M. Duda, X.-Y. Huang, W. Wang, and J. G. Powers (2008), A description of the Advanced Research WRF Version 3, technical note, Natl. Cent. for Atmos. Res., Boulder, Colo.

Stocks, B. J., et al. (1998), Climate change and forest fire potential in Russian and Canadian boreal forests, *Clim. Change*, *38*(1), 1–13, doi:10.1023/A:1005306001055.

Stohl, A. (2006), Characteristics of atmospheric transport into the Arctic troposphere, *J. Geophys. Res.*, *111*, D11306, doi:10.1029/2005JD006888.

Stohl, A., et al. (2006), Pan-Arctic enhancements of light absorbing aerosol concentrations due to North American boreal forest fires during summer 2004, *J. Geophys. Res.*, *111*, D22214, doi:10.1029/2006JD007216.

Stohl, A., et al. (2007), Arctic smoke—Record high air pollution levels in the European Arctic due to agricultural fires in Eastern Europe in spring 2006, *Atmos. Chem. Phys.*, *7*(2), 511–534, doi:10.5194/acp-7-511-2007.

Tomikawa, Y., and K. Sato (2005), Design of the NIPR trajectory model, *Polar Meteorol. Glaciol.*, *19*, 120–137.

Treffeisen, R., et al. (2007), Arctic smoke—Aerosol characteristics during a record smoke event in the European Arctic and its radiative impact, *Atmos. Chem. Phys.*, *7*(11), 3035–3053, doi:10.5194/acp-7-3035-2007.

Warneke, C., et al. (2004), Comparison of daytime and nighttime oxidation of biogenic and anthropogenic VOCs along the New England coast in summer during New England Air Quality Study 2002, *J. Geophys. Res.*, *109*, D10309, doi:10.1029/2003JD004424.

Warneke, C., et al. (2006), Biomass burning and anthropogenic sources of CO over New England in the summer 2004, *J. Geophys. Res.*, *111*, D23S15, doi:10.1029/2005JD006878.

Warneke, C., et al. (2009), Biomass burning in Siberia and Kazakhstan as an important source for haze over the Alaskan Arctic in April 2008, *Geophys. Res. Lett.*, *36*, L02813, doi:10.1029/2008GL036194.

Warneke, C., et al. (2010), An important contribution to springtime Arctic aerosol from biomass burning in Russia, *Geophys. Res. Lett.*, *37*, L01801, doi:10.1029/2009GL041816.

Wisthaler, A., A. Hansel, R. R. Dickerson, and P. J. Crutzen (2002), Organic trace gas measurements by PTR-MS during INDOEX 1999, *J. Geophys. Res.*, *107*(D19), 8024, doi:10.1029/2001JD000576.

Xie, P., and P. A. Arkin (1997), Global precipitation: A 17-year monthly analysis based on gauge observations, satellite estimates, and numerical model outputs, *Bull. Am. Meteorol. Soc.*, *78*, 2539–2558, doi:10.1175/1520-0477(1997)078<2539:GPAYMA>2.0.CO;2.

Yamanouchi, T., et al. (2005), Arctic Study of Tropospheric Aerosol and Radiation (ASTAR) 2000: Arctic haze case study, *Tellus, Ser. B*, *57*(2), 141–152, doi:10.1111/j.1600-0889.2005.00140.x.

D. R. Blake, Department of Chemistry, University of California, Irvine, CA 92697-2025, USA. (drblake@uci.edu)

G. Diskin, NASA Langley Research Center, Hampton, VA 23681, USA. (glenn.s.diskin@nasa.gov)

H. E. Fuelberg and W. R. Sessions, Department of Meteorology, Florida State University, Tallahassee, FL 32306-3034, USA. (hfuelberg@fsu.edu; walter.sessions@gmail.com)

M. Koike, Department of Earth and Planetary Science, Graduate School of Science, University of Tokyo, Hongo 7-3-1, Bunkyo-ku, Tokyo 113-0033, Japan. (koike@eps.s.u-tokyo.ac.jp)

Y. Kondo, H. Matsui, N. Moteki, and N. Takegawa, Research Center for Advanced Science and Technology, University of Tokyo, 4-6-1 Komaba, Meguro-ku, Tokyo 153-8904, Japan. (y.kondo@atmos.rcast.u-tokyo.ac.jp; matsui@atmos.rcast.u-tokyo.ac.jp; moteki@atmos.rcast.u-tokyo.ac.jp; takegawa@atmos.rcast.u-tokyo.ac.jp)

L. K. Sahu, Physical Research Laboratory, Navarangpura, Ahmedabad 380009, India. (lokesh@prl.res.in)

A. Wisthaler, Institute of Ion Physics and Applied Physics, University of Innsbruck, Technikerstrasse 25, A-6020 Innsbruck, Austria. (armin.wisthaler@uibk.ac.at)

Y. Zhao, Air Quality Research Center, University of California, One Shields Ave., Davis, CA 95616, USA. (yjzhao@ucdavis.edu)